Tracing lake pollution, eutrophication and partial recovery from the sediments of Windermere, UK, using geochemistry and sediment microfabrics

J. James Fielding[1, 3], Ian W. Croudace[1], Alan E. S. Kemp[1], Richard B. Pearce[1], Carol J. Cotterill[2], Peter Langdon[3], Rachael Avery[1, 4]

Authors final accepted manuscript

Published in Science of the Total Environment 722 (2020) 137745

doi.org/10.1016/j.scitotenv.2020.137745

[1]Ocean and Earth Science, University of Southampton, National Oceanography Centre, Southampton, SO14 3ZH, United Kingdom

[2]British Geological Survey, Lyell Centre, Research Avenue South, Edinburgh, United Kingdom EH14 4AP

[3] School of Geography and Environmental Science, University of Southampton, University Road, Southampton, SO17 1BJ

[4]Department of Geological Sciences, Stockholm University, SE-10691, Stockholm, Sweden

*corresponding author (jj1n19@soton.ac.uk)

Abstract

Many lakes undergo anthropogenically driven eutrophication and pollution leading to decreased water and sediment quality. These effects can enhance seasonally changing lake redox conditions that may concentrate potentially toxic elements. Here we report the results

of a multi-method geochemical and sediment microfabric analysis applied to reconstruct the history of cultural eutrophication and pollution of the North and South Basins of Windermere, UK. Eutrophication developed from the mid-19th to the earliest 20th centuries. Enhanced lake productivity is indicated by increased sedimentary $\delta^{13}C$, and increased pollution by a higher concentration of metals (Pb, Hg, and As) in the sediment, likely enhanced by incorporation and adsorption to settling diatom aggregates, preserved as sedimentary laminae. In the South Basin, increasing sediment $\delta^{15}N$ values occur in step with Zn, Hg, and Cu, linking metal enrichment to isotopically heavy nitrate (N) from anthropogenic sources. From around 1930, decreases in Mn and Fe-rich laminae indicate reduced deep-water ventilation, whereas periods of sediment anoxia increased, being most severe in the deeper North Basin. Strongly reducing sediment conditions promoted Fe and Mn reduction and Pb-bearing barite formation, hitherto only described from toxic mine wastes and contaminated soils. From 1980 there was an increase in indicators of bottom water oxygenation, although not to before 1930. But in the South Basin, the continued impacts of sewage is indicated by elevated sediment $\delta^{15}N$. Imaging and X-ray microanalysis using scanning electron microscopy has shown seasonal-scale redox mineralisation of Mn, Fe, and Ba related to intermittent sediment anoxia. Elevated concentrations of these metals and As also occur in the surficial sediment and provide evidence for dynamic redox mobilisation of potentially toxic elements to the lake water. Concentrations of As (up to 80 ppm), exceed international Sediment Quality Standards. This process may become more prevalent in the future with climate change driving lengthened summer stratification.

Key Words: paleolimnology, multi-method, cultural eutrophication, Itrax XRF core scanning, isotopic analysis, scanning electron microscopy.

1. Introduction

Freshwater lakes represent a critical resource providing a wide range of services, such as a municipal water sources (Fowler et al., 2007), flood mitigation (Thampapillai and Musgrave, 1985), habitats for rare and protected species (Dudgeon et al., 2006; Maberly and Elliott, 2012), and are often the basis for a multi-million-pound tourism industry (Maltby et al., 2011). Despite their value, many are poorly managed and subject to anthropogenic stressors, such as cultural eutrophication caused predominantly by phosphorus (P) and nitrogen (N) enrichment (Richardson and Jørgensen, 1996), and toxic metal enrichment, from industrial and municipal pollution (Förstner and Wittmann, 2012). The consequent economic impact is estimated to be £ 75 -115 M yr^{-1} in England and Wales alone (Harvey et al., 2012; Pretty et al., 2003). Furthermore, anthropogenic climate change has been linked to amplification of these stressors (Williamson et al., 2009), making the restoration of freshwater lakes a priority (Gulati et al., 2012). To this end, current legislation (the European Union Water Framework Directive, WFD; 2000/06/EC) legally obliges stakeholders to return waterbodies to "a good ecological and chemical status" with reference to pre-anthropogenic chemical, ecological and environmental conditions (Carvalho et al., 2019).

Numerous lakes in industrialised areas or near developing population centres have undergone similar histories over the past 1-2 centuries with progressive eutrophication and pollution driven by population increase, agricultural intensification and industrialisation (Dudgeon et al., 2006; Hodell and Schelske, 1998). Despite more recent remediation measures, anthropogenic activities have often left a legacy of sediments enriched in metals and trace elements (Thevenon et al., 2011). Many lakes vary seasonally with summer stratification allowing depletion of oxygen in the hypolimnion that may lead to anoxia in the bottom sediments. Such seasonal-scale redox changes may affect the absorption or release of pollutants, potentially producing relatively high concentrations on the lake bed or in the lake waters (Itai et al., 2012; Wu et al., 2017). Climate change may reinforce such processes

since raised temperatures may lead to a longer and more intense stratification period driving enhanced isolation of bottom waters (Jenny et al., 2014). In order to reconstruct the history of lake eutrophication and to assess the efficacy of lake restoration programmes, it is necessary to obtain detailed geochemical records of lake sediments to quantify the history of inputs and to investigate the controls on mineral formation and dissolution (Thevenon et al., 2011; Wu et al., 2017).

In this context, Windermere, England's largest natural lake, has undergone a typical trajectory of pollution and eutrophication over the past 150 years (McGowan et al., 2012; Moorehouse et al., 2014; 2018). This has been recorded, in part, by regular monitoring of the water column since the 1940s (Pickering, 2001; Maberly et al., 2011), however, the extent to which anthropogenic pollution has affected the lake beyond the time scale of monitoring and how the lake sediments are affected are not yet fully understood. Windermere forms a particularly interesting case study as it comprises two basins which are variably susceptible to eutrophication, which together, constitute a sensitive barometer to the effects of anthropogenic and climatic influences (Pennington, 1973; McGowan et al. 2012).

This study has applied a range of geochemical and sediment fabric techniques to reconstruct the history of anthropogenic impacts on Windermere. By combining radiochronology, major and trace element geochemistry and high resolution scanning electron microscope sediment microfabric imaging on new gravity cores, we reconstruct the sedimentary history including the input of metals and toxic elements and the relation to biological activity and redox changes in the lake sediment. Sediment fabric analysis specifically enables us to relate anthropogenically-induced pollution and eutrophication to biological activity, including the reconstruction of seasonal-scale algal blooms in the lake surface waters and of the activity of zoobenthos on the lake bed.

2. Study location, materials and methods

2.1. Study site

Windermere, in the Lake District National Park, (Fig. 1), is of particular significance as it acts as a refugium for locally rare fish species such as the Arctic Char (Winfield et al. 2008; Miller et al., 2015), a municipal water supply for the North West of England during periods of drought, and is host to a thriving tourist industry. The lake is 17 km long with a maximum width of 1.5 km and is divided into a North Basin (maximum depth 64 m) and a South Basin (maximum depth 42 m) separated by an area of basement high, small islands and shallows with an average depth of 10 m (Pearsall and Pennington, 1973; Pickering, 2001; Miller *et al*, 2013). The larger North Basin has a surface area of 8.1 km2 and volume of 201.8 x 10^6 m^3 while the South Basin has a surface area of 6.7 km^2 and volume just over half that of the North at 112.7 x 10^6 m^3 (McGowan et al., 2012). The main freshwater inflows are from the rivers Rothay and Brathay (Fig. 1). Primary inflow to the South Basin comes from the North Basin and from Cunsey Beck that drains the small seasonally anoxic lake, Esthwaite Water. Outflow is at the south end via the River Leven (Fig. 1), with retention times in the North and South Basin of 180 and 100 days respectively (Moorhouse et al., 2018).

The lake is currently classified as warm monomictic (Hutchinson and Löffler, 1956), becoming stratified in early summer with re-mixing usually in late October or early November in the South Basin and a later (November or December) in the North Basin (Pickering, 2001). The water column has been regularly monitored and sampled for its physical properties, chemistry and biology since 1945 by the Freshwater Biological Association (FBA) and the Centre for Ecology and Hydrology (CEH) (Reynolds and Irish, 2000; Pickering, 2001; McGowan et al., 2012). These records show a progressive mid- to late-20^{th} century increase in eutrophication, especially in the South Basin (Reynolds and Irish,

2000). The current trophic status of the North Basin is mesotrophic and that of the South Basin, eutrophic (Moorhouse et al., 2018). Palaeolimnological studies of the sediments of Windermere indicate a mid- to late-19th century onset for eutrophication driven primarily by population increase (Pennington, 1973; Sabater and Howarth, 1995, McGowan et al., 2012), marked in the sediment by the transition from "brown mud" to a "black ooze" (Pennington, 1973; Sabater and Howarth, 1995). Enrichments in some metals (Pb, Zn, Cu) were previously reported within the "black ooze" from cores taken in the South Basin in 1975 (Hamilton-Taylor et al., 1984). A more recent geochemical study of piston cores taken from Windermere in 2012 found a 20th century enrichment in metals (Miller et al., 2014), but did not recover the topmost 10–20 cm of sediment.

2.2. *Core location, sampling and analysis*

Following the bathymetric surveys and coring reported in Miller et al. (2013), the four gravity cores of the present study were taken in 2014 from mid-depths and deep basinal locations (Fig. 1), recovering the sediment-water interface and up to 46 cm of sediment (Table 1). The cores were split at the British Ocean Sediment Core Facility (BOSCORF), then processed and sampled using standard methods for high resolution sediment fabric analysis (Dean et al., 1999; Kemp et al., 2001). Split cores underwent digital imaging, x-radiograph imaging and geochemically analysis using an Itrax Energy Dispersive X-Ray Fluorescence (ED-XRF) core scanner (Croudace et al., 2006). To calibrate and complement the ED-XRF analyses, continuous sediment samples (1 cm resolution) were also analysed by Wavelength Dispersive XRF Spectrometer. Mercury was measured using a Milestone DMA-1 system (Milestone SRL, Italy) employing sample thermal decomposition, mercury amalgamation and atomic absorption detection providing a typical detection limit in the ppt range. Further details of the methods are found in the Supplementary Material.

142 *2.2.1. Microfabric analysis*

143 One centimetre-thick slab samples were taken continuously with overlapping sections for
144 microfabric studies. These slabs were X-rayed, and following further subsampling,
145 underwent fluid-displacive resin embedding after which covered thin sections (CTS) for
146 optical microscopy and polished thin sections (PTS) for backscatter electron imagery were
147 prepared. PTS were imaged and analysed using a Scanning Electron Microscope (SEM).
148 Sediment fabrics, including bioturbation and mineral and organic components, were
149 documented using a combination of photomosaic and higher magnification backscatter
150 electron images (BSEI), together with optical thin section microscopy. For further analysis of
151 microfossil remains and mineral habits and structures, SEM stub samples were prepared
152 from the un-treated sediment counterparts to the embedded sediment sections.

153 To match broader scale variations in geochemistry with changes in sediment microfabric
154 and mineralogy, elemental maps, line scans, and spot analyses of key intervals within PTS
155 were undertaken in the SEM by energy dispersive X-ray spectroscopy microanalysis (EDS).

156 *2.2.2. TOC, TN, $\delta^{13}C$*

157 One gram samples, taken continuously at 2 cm intervals from cores SC68 and SC57 were
158 analysed for TOC, TN, $\delta^{13}C$ and $\delta^{15}N$ using a Elementar Vario Isotope Cube Elemental
159 Analyser equipped with a TCD (Thermal conductivity detector), interfaced with an isotope
160 ratio mass spectrometer (IRMS). Six samples representing sediment endmember types in
161 both basins were tested for calcium carbonate ($CaCO_3$), and all yielded results below the
162 detection limit (4 counts).

163 **2.3. Chronology**

164 *2.3.1. ^{210}Pb and ^{137}Cs*

One centimetre thick samples were taken at regular intervals and analysed for ^{210}Pb and ^{137}Cs in all cores. ^{137}Cs was measured by direct gamma spectrometry using a Canberra well-type HPGe gamma-ray spectrometer counting for 100,000 seconds and evaluating the 661 keV photopeak (Croudace et al., 2012; Ritchie and McHenry, 1990). Gamma spectra were processed using FITZPEAKS gamma deconvolving software (JF Computing, Stanford in the Vale, UK). Each activity was corrected for sample mass and volume. Lead-210 was measured (via its granddaughter Po-210) using a method based on Flynn (1968) involving double acid leaching, ^{209}Po spiking and auto-deposition onto silver discs to determine ^{210}Pb activities using alpha spectrometry (Croudace et al., 2012). The linear sedimentation accumulation rates (LSR) and subsequent age estimates reported below are generated from ^{210}Pb activity and validated using ^{137}Cs.

A chronology was generated from excess ^{210}Pb (^{210}Pbxs) activity data for the top of each gravity core by applying the constant flux: constant sedimentation (CF:CS) model (Robbins, 1978). The model generates an LSR that is extrapolated down core (Fig. 2). Age error was calculated by applying the CF:CS model to the upper and lower counting statistical uncertainty of ^{210}Pbxs values to produce LSRs which were extrapolated down core to give an upper and lower age depth error estimate. All ^{210}Pb ages stated in this paper are given in years A.D. and are the median probable ages followed by instrument uncertainty–in brackets. LSR generated from ^{210}Pb were only applied to depths at which ^{210}Pbxs activity exceeded the background concentration. Below this, age estimates were generated by linear interpolation of the model to the topmost radiocarbon age in the corresponding piston core. Accumulation rates based on ^{137}Cs used the depths of initial increase of the 1963 bomb peak from atmospheric nuclear weapons testing and the Chernobyl nuclear reactor incident (1986) (Ritchie and McHenry, 1990).

2.3.2. Radiocarbon dating

In 2012 piston cores were taken at the same locations as the gravity cores (Avery et al., 2017). From these split core surfaces a series of samples were taken for ^{14}C analysis following an inspection of the core for macrofossils, and analysed by the Natural Environment Research Council Radiocarbon Facility (NRCF) in East Kilbride. In order to extend the age-depth model beyond the oldest date achievable by ^{210}Pb and ^{137}Cs the uppermost ^{14}C analyses from the piston cores (Table 2) were used. Integration of the gravity and piston core age depth, and overlap at corresponding sites was achieved by matching lithostratigraphy, ^{210}Pb and ^{137}Cs data from both cores. Samples from the piston cores were for radiocarbon analysis were converted to graphite and processed at the Scottish Universities Environmental Research Centre (SUERC) laboratory for accelerator mass spectrometry (AMS) ^{14}C analysis (Damon et al., 1989).

Radiocarbon dates were processed and calibrated using Calib 7.1 (Stuiver and Reimer, 1993) and the Intcal 13 calibration curve (Reimer et al., 2013). The radiocarbon results are reported with ages given as the calibrated median probability age, and 2σ calibrated ages.

3. Results

3.1. Age-depth model

The age-depth model and LSR generated from ^{210}Pb and ^{137}Cs data for the upper part of the cores (SC68 = 27cm, SC64 = 20.5cm, SC67 = 18.5cm, SC57 = 22.5cm) is described in detail in Fielding et al. (2018). In all cores linear interpolation between the deepest ^{210}Pb activity and the upper most radiocarbon date in the corresponding piston cores (Table 2) yielded LSR an order of magnitude lower than those generated by the CF:CS model in the upper part of the core. This increase in sedimentation since the 19th century is consistent with other studies in the area, and could have a number of causes including increases in land erosion due to

214 agriculture and increases in biogenic sediment as a result of increased primary productivity
215 in the lake (Sabater and Haworth, 1995; Schillereff et al., 2019).

216 **3.2. Lithostratigraphy and Geochemistry**

217 The North Basin cores comprise a lower pale brown mud (Unit I) overlain by a dark grey
218 mud (Unit II), a thin pale clay rich interval (Unit III) and an upper pale brown mud (Unit IV)
219 (Fig. 3). The South Basin stratigraphy is similar, except that Unit III is missing and the upper
220 muds of Unit IV are darker in Core 57 (Fig. 4). This stratigraphy is broadly consistent with
221 earlier cores taken from Windermere with the "brown mud" of Pennington (1973) and
222 Sabater and Howarth (1995) corresponding to Unit I and their "black ooze" to our Unit II.
223 The main difference is the thicker upper pale brown mud, our Unit I, reflecting an additional
224 3–4 decades of recent sediment accumulation, the transition to Unit I having been around
225 1970–1975. The thin clay-rich interval in the North Basin (Unit III) is interpreted as an event
226 bed generated by a slope failure restricted to the North Basin caused by the 1979 Carlisle
227 earthquake (Fielding et al., 2018; Musson and Henni, 2002). The transition from Unit I to
228 Unit II occurs earlier in the deep South Basin cores (1870 in SC67; 1883 in SC57) than in those
229 from the North Basin (1916 in SC64; 1920 in SC68).

230 Major and trace element variability are presented in Figs. 3, 4 and supplementary Figs. 1 – 4,
231 and total carbon and nitrogen and stable isotopes $\delta^{13}C$ and $\delta^{15}N$ in Fig. 5. These results are
232 discussed in section 4 below in the context of the overall pollution and eutrophication
233 history of Windermere. Details of the geochemical microfabrics and barium mineralogy
234 encountered are given below.

235 **3.3. Sediment fabrics and preservation of lamination**

236 *3.3.1. Sediment microfabrics and lamina types*

237 Microfabrics vary from laminated through homogeneous and unstructured sediment to
238 pervasively pelleted, with pellets ranging in size between 50- 350μm, (Fig. 6). Terrigenous
239 silty clays (Fig. 6c) form the dominant sediment type and are interspersed with a more
240 porous sediment (PS) type (paler in optical microscopy/ darker in BSEI) (Fig. 6b),
241 comprising silty clay and organic material. Fe and/or Fe and Mn minerals typically occur
242 within porous sediment laminae, for example in Unit I of SC68 and in near surface sediment
243 (Fig. 6b). The silty clays of Unit II are distinctly dark-coloured under optical microscopy
244 (Fig. 6d).

245 Obvious lamination comparable to regular varves (Zolitschka et al., 2015) was rarely
246 observable directly on the split core surfaces. However, a combination of optical microscopy
247 and BSEI of embedded sediment reveals a range of lamina types, the most common being
248 0.8 – 5.5 mm thick and comprising alternations of detrital terrigenous and higher porosity
249 laminae with the latter often containing autochthonous organic material laminae and
250 reduced detrital content (Figs 5c). The high porosity laminae also often contain enrichments
251 of Fe or both Fe and Mn minerals (see 3.4.1, below).

252 *3.3.2. Diatom ooze laminae*

253 Microlithostratigraphic analysis shows that Units II and IV are abundant in diatom remains.
254 In SC68, diatoms are concentrated in distinct laminae ranging in thickness from 0.2 to 1 mm
255 (Fig. 7). Twelve diatom ooze laminae occur in SC68 and a single lamina is present in SC64.
256 The greater preservation of laminae in SC68 reflects its deep basin location that would be
257 more prone to anoxia (see 4.3.3, below). Imaging of stub samples taken from the laminae
258 reveals that they are composed of near-monospecific concentrations of *Asterionella formosa* in
259 Unit II, and *Aulacoseira subarctica*, in Unit IV (Fig. 7).

260 **3.4. Geochemical fabrics**

3.4.1. *Fe- and Mn-rich laminae*

Fe and/or Mn minerals typically occur within porous sediment laminae, for example in Unit I of SC68 and in near surface sediment (Fig. 6b). Enrichments in Fe and Mn occur intermittently in all the cores but are most abundant in Unit I of the deep North Basin (SC68) (Fig. 3). Peaks in Mn in the lower laminated sediments were associated with concentrations of a rhombohedral mineral which was identified as rhodochrosite ($MnCO_3$) by EDS elemental mapping and line scans (Fig. 8). The rhodochrosite occurs as both individual crystals with a typical size range of 2–10 μm, but also as dense clusters of crystals, up to 60 μm across (Fig. 8A). Mn peaks in the upper core interval are not associated with rhodochrosite, but rather with amorphous Mn oxyhydroxides. Fe peaks throughout the sediments were shown to be associated with authigenic amorphous and crystalline iron (oxy)hydroxide (Fe(O)OH), most likely lepidocrocite, occurring as subhedral platy agglomerates ranging in size from between 50 μm to 700 μm (Fig. 8B).

Selected intervals were investigated with EDS elemental mapping and line scans (Fig 9). To indicate variation in detrital sediment, Si is also shown. Decreases in Si coincide with increases in Mn and or Fe in the more porous laminae, they are also indicated by paler zones in the thin section photomicrographs (Fig. 9). In some cases, the laminae appear in pairs separated by terrigenous-rich laminae, with the Mn lamina located above or overlapping with the Fe-rich lamina (Fig. 9a, c). In this instance the laminae are distinct on the EDS maps and line scans despite pelletisation. In other cases, the order is less clear (Fig. 9) although the Mn enrichment (0.05 to 2.2 mm thick) generally occur towards the upper part of the Fe-enrichment (0.2 to 3 mm thick) while in some cases only Fe enrichments (0.1 to 1 mm thick) occur (Fig. 9). The mineral rich-detrital rich laminae couplets range between 0.14 and 0.8 cm in thickness with an average of 0.24 cm. Given the LSR of 0.29 cm/ yr^{-1} for this Pb-dated section of the core, a quasi-annual occurrence is plausible for the upper intervals.

3.4.2. Barium mineralogy

Barium (Ba) content is marked in all cores, except SC68, by peak values near the sediment water interface (SWI), with maximum values of up to 0.2 wt% in core SC57. Below this there are smaller increases above the clay horizon in the North Basin cores, SC64 and SC68 and there is elevated Ba content within the upper part of Unit II in SC68 and SC67. In SC68 Ba also shows high variability at the base of the core. SEM examination of sediment reveals the common presence of small, typically 2–12 μm-sized crystals of barite that may occur in clusters or individually. SEM EDS analysis indicates that these have a normal barite $BaSO_4$ composition near the core top, but within Unit IV they contain Pb and so are on the Barite ($BaSO_4$)-Anglesite ($PbSO_4$) solid solution series (Fig. 10). The barite-anglesite crystals are most abundant in SC57 and SC64 but occur in all cores and increase in abundance in the mid and upper part of Unit IV. Here microlithostratigraphic analysis shows the presence of $BaSO_4$ in the SWI appearing as individual euhedral minerals up to 5 μm and in clusters up to 35 μm.

4. Discussion

4.1. Causes and significance of pelleting

In lake waters deeper than 20 m, pelletal structures (50–300 μm) are produced mainly by conveyer-belt feeding tubificid oligochaetes or by chironomid larvae (McCall and Tevesz, 1982). Both mechanisms can cause vertical redistribution of sediment but usually over very small distances (2–9 cm). In Windermere it was found that vertical redistribution by bioturbation was limited to 1.5 cm (Fielding et al., 2018) and that while this disrupted the original sediment structure in some places it did not completely remove it. The presence of pellets does not, however, necessarily imply sustained oxic conditions since oligochaetes such as *Tubifex* spp. are known to survive in anoxia (Famme and Knudsen, 1985) and have

been observed in abundance in the profundal sediments of Windermere even with seasonally anoxic bottom water conditions (Reynoldson, 1987). Furthermore, some chironomids contain haemoglobin, and as such can survive in anoxic conditions through a range of respiration strategies (Brodersen, 2008). In this instance, therefore, it is the extent of pelletisation that is likely related to the relative degree and persistence of sediment anoxia, since the overall benthic activity would be inhibited during prolonged anoxia (Reynoldson, 1987).

4.2. Use of Mn and Fe content and mineralogy as redox indicators

Mn and Fe are sensitive redox indicators since both metals have soluble reduced ions but on oxidation form solid oxyhydroxides (Davison, 1993). There are two circumstances in which Mn and Fe minerals may be used to reconstruct ventilation histories in lakes. In lakes with anoxic bottom waters, the dissolved ions of Fe and Mn are present. In such lakes, for example, Lake Zurich, seasonal ventilation of bottom waters and the introduction of oxygen leads to the formation and subsequent sedimentation of solid phase Fe- and Mn- oxyhydroxides that may preserve a record of ventilation events in seasonally laminated sediments (Naeher et al., 2013). In these cases, laminae of Fe/Mn minerals record lake ventilation events. On the other hand, in lakes without persistent anoxia, consumption of oxygen in the hypolimnion during the summer-autumn stratification period promotes sediment anoxia and leads to mobility of Fe and Mn ions. In this case Fe and Mn will precipitate at a redox boundary, either within the sediment (as is the case in Lake Baikal; Och et al., 2012) or at the sediment water interface (SWI) as pore waters interact with oxygenated bottom waters (Schaller et al., 1997). From monitoring of Windermere, hypolimnetic anoxia has only been recorded in the deepest part of the South Basin late in the stratified summer period occasionally between 1979 and 1991 during the period of peak eutrophication (Hamilton-Taylor and Willis, 1990; Pickering, 2001). The presence of Fe or Mn layers in Windermere sediments (Figs. 3, 4, 9), therefore, records periods where reduced bottom water oxygenation led to reduced oxygen in the upper sediments, and a shallowing of the

oxycline in the sediment, facilitating the mobility of Fe and Mn and their subsequent oxidation at or near the SWI (Fig. 3). The occurrence of Fe laminae without overlying Mn concentrations (Fig. 9) indicates that some overturning episodes were not of sufficient duration or intensity to allow the slower-oxidising Mn to precipitate suggesting release of Mn to the water column. In scenarios where reducing conditions in the sediment result in the dissolution of Mn oxyhydroxides there may still be the potential to preserve a record if rhodochrosite is formed (Yu et al., 2016) as was evidently the case in Unit IV of SC68. The distribution and variability in Fe and Mn may therefore be used to reconstruct the Windermere sediment redox history.

4.3. The sedimentary record of the pollution and eutrophication of Windermere

4.3.1. Asynchrony between the South and North Basin

The increase in metals (Pb, Zn, Cu) and As in the North Basin occurs around 1910–1920, lagging the appearance in the South Basin by around 70–100 years for Pb and 30 years for Zn, Cu and As (Figs. 3, 4; Supplementary Figs. 1-4). This lag in delivery to the North Basin is unlikely to be due to differences in the sources of metals (sewage and atmospheric), as this would have occurred almost synchronously on a catchment to regional scale. Instead, it may be that the efficient delivery of the metals to the sediment was enhanced by increased algal productivity and scavenging during flux. For example, sediment trap studies from Windermere show take up of Zn by diatoms (Reynolds and Hamilton-Taylor, 1992) and enrichments of both Zn and Pb were found associated with the eutrophic-indicating diatom *Asterionella formosa* (Lund, 1957). Furthermore, the extracellular polymeric substances (EPS) exuded by both diatoms and associated bacteria in lake "snow" aggregates (Schweitzer et al., 2001) are also efficient scavengers of trace metals (Bhaskar and Bhosle, 2006; Comte et al., 2008). The smaller water volume of the South Basin makes it more susceptible to enrichment and eutrophication than the North Basin and it also receives a higher nutrient load (Pickering, 2001), so that the earlier increase in metals may be related to the earlier increases

in algal productivity and associated scavenging from the water column. There is also a similar lag in the $\delta^{15}N$ of organic matter that is consistent with the earlier eutrophication in the South Basin. Such earlier productivity increases in the South Basin are also recorded in algal pigment records with South Basin production increasing markedly from around 1860 and that of the North Basin increasing more gradually from 1890 to highs from around 1940 (McGowan et al., 2012).

4.3.2. 1800–1940: The onset and increase in pollution

Increases in Pb content in the early to mid- 19th century in the South Basin (SC67–1810s; SC57–1850s) and from around 1910–20 in the North Basin represent the first significant signs of anthropogenic contaminants in the sediment. Although there was considerable mining and quarrying for metals in the North of the Windermere catchment in the 19th century, the periods of metal extraction do not coincide with increases in metal content in the lake sediment (Miller et al., 2014). Double-spike Pb isotope analysis of Windermere sediments dating from the 1840s to the 1920s reveals a likely Pb source to be from Carboniferous coal, related to the launch of coal-fired steam ships from 1845 and the further expansion of their use following the opening of the Kendall-Windermere railway in 1847 (Fig. 11) (Miller et al., 2014). The increase in Pb prior to other metals is also recorded in the sediments of the adjacent Blelham Tarn (Ochsenbein et al., 1983). The increased use of petroleum in road vehicles is also a significant contributor of Pb from 1920 onward (Miller et al., 2014).

The increase in the other metals (Zn, Cu, Hg; Supplementary Figs. 1-4) and As from 1880–1990 and concomitant darkening of the sediment in the South Basin (Fig. 4), coincides with increased sewage discharge from the rapidly increasing population centres around the lake (McGowan et al., 2012) and this is consistent with previous metal studies in Windermere (Hamilton-Taylor and Willis, 1990). High levels of As and Hg persisted in the South Basin

385 from the 1920s through the following six decades. Increasing values of the $\delta^{15}N$ of organic
386 matter in the South Basin sediment also occur from around 1890 (SC57), in step with the
387 metals (other than Pb) from this time. In the North Basin, by contrast, a prominent increase
388 in $\delta^{15}N$ of organic matter together with metals does not occur until the 1930s (Figs 3, 13,
389 Supplementary Figs 1, 2). Elevation in $\delta^{15}N$ of organic matter can be attributed to a number
390 of causes including increased algal productivity (Hodell and Schelske, 1998) or the input of
391 isotopically heavy nitrate from primary sewage or farm runoff (Meyers, 1994; Moorhouse et
392 al., 2018). Although, in Windermere all of these may be applicable, recent analysis shows
393 that lake primary producer variability tracks modifications to waste water treatment works
394 in both the North (~65% variance explained) and South Basins (~62% variance explained)
395 (Moorhouse et al. 2018). The darkening of the sediment also coincided with the first rise to
396 prominence of the eutrophic-indicating diatom *Asterionella formosa* (Sabater and Haworth,
397 1995) (Figs 7, 12). Elevated productivity in both basins is also evidenced by increasing $\delta^{13}C$
398 values of organic matter through the 19th and early 20th centuries (Fig. 5). Phytoplankton
399 preferentially take up the lighter ^{12}C isotope during photosynthesis, but in periods of
400 sustained high productivity they will increasingly utilise the heavier isotope resulting in an
401 increase in $\delta^{13}C$ values (Schelske and Hodell, 1995). The increase in $\delta^{13}C$ values in
402 Windermere is consistent with steadily increasing algal productivity during this period. The
403 $\delta^{13}C$ values are around 1‰ heavier in the South Basin, possibly reflecting its greater
404 susceptibility to eutrophication due to its smaller volume, although phytoplantonic species
405 composition or organic matter source changes could also affect this (Gu et al. 1999). While
406 there is broad agreement with $\delta^{13}C$ values from an earlier Windermere core study
407 (McGowan et al., 2012) other organic proxies (TOC, TN, C:N) show a somewhat different
408 trend. This could be due to differences in analytical methods since McGowan et al.
409 measured carbon by loss on ignition whereas we used an elemental analyser.

Regarding sediment redox conditions, the regular occurrence of Fe and Mn laminae in the deep North Basin (SC68 – 54 m water depth) prior to the 19th century indicate intermittent sediment anoxia, but with regular deep-water ventilation in the period prior to eutrophication. When compared to the LSR of the core (<27.5 cm depth: 0.29 cm yrs^{-1}, >27.5 cm depth: 0.04 cm yrs^{-1}) the regular spacing of these mineral laminae (Fig. 3) (0.2–0.7 cm) suggests these features represent redox changes, and resulting deposition of Mn and or Fe, occurring on annual to multi-annual scale (Fig. 9a). The pattern is consistent with summer stratification and a reduction in bottom water oxygenation that promoted anoxia in the sediment and allowing the release and upwards diffusion of dissolved Fe and Mn ions. This would have been followed by lake turnover in the autumn/ winter that led to re-oxygenation of bottom waters and formation of the Fe and Mn oxides that precipitated at a redox boundary within the surficial sediment. The occurrence of rhodochrosite rather than Mn oxyhydroxides suggests that reducing conditions in the sediment may have driven dissolution of the oxyhydroxides, but that the Mn subsequently combined with carbonate (Yu et al., 2016). The less frequent occurrence of Fe laminae and presence of only a single Mn lamina in SC64 is consistent with its location in shallower waters (26m) which remain oxygenated for longer than deeper waters in the hypolimnion. Here, the occasional Fe and Mn laminae represent periods where sufficient dysoxia occurred in even the shallower waters, followed by reoxygenation resulted in the concentrating of redox sensitive elements in the sediments.

As the colour changes from pale brown to grey (Unit I to II) in the 1920s these Fe and Mn laminae become progressively less abundant until they cease, with the slower oxidising Mn disappearing first. The concomitant decrease in the extent of pelletisation of the sediment is also consistent with progressively increasing bottom water hypoxia and sediment anoxia (Fig. 3). Combined with the cessation of Mn oxyhydroxide preservation and the lack of

pelletisation in the shallower SC64, this suggests increasing incidence and persistence of sediment anoxia in the North Basin (Fig. 3).

4.3.3. 1940–1980: Peak pollution and eutrophication, sediment anoxia and bottom water hypoxia

Sustained high concentrations of metals were present in both basins from around 1940 coinciding with further darkening of the sediment, high levels of sediment organic carbon and persistent high values of the $\delta^{15}N$ of organic matter. This was likely driven by an increase in resident population during World War II that eventually overwhelmed the existing sewage treatment facilities at Tower Wood (McGowan et al., 2012) leading to increased sewage discharge to the lake. In addition, following WW II the application of N rich artificial fertiliser significantly increased UK wide (McGowan et al., 2012) making agricultural run off another likely driver of persistent high values of the $\delta^{15}N$.

In both basins, peak organic carbon contents occurred from 1950–1980 and this also coincides with some of the highest $\delta^{13}C$ values marking peak productivity (Fig. 5). Lake monitoring during this period recorded blooms dominated by the diatom *Asterionella formosa*, a characteristic indicator of eutrophication (Lund, 1972; Lund et al., 1963). These recurrent annual blooms occurred in May/ June with massive flux in late June. Close monitoring of the 1947 bloom observed a flocculent mass of cells accumulating on the surface sediment (Lund et al., 1963). From the 1940s, increasing sediment anoxia in the deep North Basin (SC68), as evidenced by a decrease in pelletisation and cessation of Fe and Mn laminae, led to the preservation of several of these layers as sedimentary laminae recording the near-monospecific nature of the *Asterionella formosa* blooms (Figs 3, 4, 7, 12), with the last preserved around 1983 (Fig. 12). Increasing diatom productivity and eutrophication was further driven by increases in soluble reactive phosphorus, particularly in the South Basin,

459 together with increases in nitrate in both basins from the mid-1960s (Reynolds and Irish,
460 2000). Sustained, elevated concentrations of metals and As occurred throughout this period
461 with peaks occurring mainly between 1950–1960.

462 During the time interval 1940–1980, peak sediment anoxia is indicated in all cores with the
463 most persistent in the deep North Basin (SC68). The presence of Fe and Mn laminae and
464 decrease in pelletisation in SC67 (1960–1980) indicate that enhanced sediment anoxia also
465 extended to shallower zones of the lake at this time. Intermittent Fe laminations in the deep
466 South Basin (SC57) are consistent with sediment anoxia developing reducing conditions
467 sufficient to mobilise both Fe and Mn but with insufficient bottom water re-ventilation to re-
468 oxidise the Mn. This sediment evidence is consistent with observations of seasonally
469 declining oxygen concentrations in the summer-autumn hypolimnion (Talling and Heaney,
470 1988) and episodic bottom water anoxia recorded in the deep South Basin from 1979
471 (Pickering, 2001). In fact, elevated Mn concentrations were observed in bottom waters
472 during late season stratification in the 1970s (Hamilton-Taylor et al., 1984; Pickering, 2001).
473 The peak sedimentary metal concentrations at this time may have been boosted by the
474 scavenging of metals by Mn- and Fe-oxides forming in the bottom waters (Hamilton-Taylor
475 and Davison, 1995; Xue et al., 1997).

476 There is no evidence of authigenic pyrite from SEM observations, so although the bottom
477 sediments were anoxic, they were rarely sulphidic and there is no evidence for sulphate
478 reduction and pyrite formation consistent with sulphur speciation studies in Windermere
479 (Davison et al., 1985). However, increases in sulphur occur in the South Basin cores in Unit II
480 (>0.5%) and all sediment cores contain frequent 2–20 μm-sized barite crystals (Fig 9). The
481 occurrence of the barite as euhedral crystals suggests a different mechanism of formation
482 from that of the adjacent seasonally anoxic Esthwaite Water, where small (3–4 μm) spherical
483 granules of barite are biologically mediated within protozoa (Finlay et al., 1983; Smith et al.,

484 2004). The origins of the Ba concentrations that led to the formation of the euhedral barite
485 crystals in Windermere may be similar to those responsible for the transfer of Ba from
486 bottom waters to the topmost sediment in Lake Biwa, Japan. Here, the hypolimnion reaches
487 minimum dissolved oxygen concentrations at the end of the stratification period in
488 December but is never totally depleted (Sugiyama et al., 1992). In this case, during the
489 period of stratification, enhanced anoxia within bottom sediments leads to the release of Fe
490 and Mn into the oxic bottom waters where they are re-oxygenated to form hydrous oxides.
491 The hydrous Mn oxides have a strong affinity for Ba which they readily scavenge and this
492 results in draw down of Ba to the sediment as the hydrous Mn oxides settle (Sugiyama et al.,
493 1992). Although water column sulphate is low in freshwater lakes, bacterial oxidation of
494 organic sulphur (Fakhraee et al., 2017) may have been important in producing the sulphate
495 for barite formation. Unlike the pure barite crystals in the near surface sediment, the crystals
496 in Unit III consistently contain Pb. The presence of barite-anglesite solid solution has not
497 been reported before from lake sediments and has primarily been associated with mining
498 waste and contaminated soils (Courtin-Nomade et al., 2008; Fernandez-Gonzalez et al.,
499 2013).

500 *4.3.4. 1980–2010: Partial Recovery*

501 From around 1980 (Units II to IV) the sediment colour changes back to pale brown in SC68
502 and SC67 and becomes less dark in SC64 and SC57. In the South Basin, decreased sediment
503 anoxia is also indicated by the resumption of pelletisation (enhanced benthic activity),
504 cessation of the Fe and Mn laminae, and decreases in sedimentary S. The decline in Pb after
505 peaks in the 1960s follows the marked decline in atmospheric Pb since peaks in the 1970s
506 (Rippey and Douglas, 2004). A post 1960s decline in metals and As in the South Basin may
507 be ascribed to the effective operation of the then newly expanded (new sedimentation tanks

508 and additional filters) Tower Wood Sewage treatment works from 1967 (Fig. 10) (McGowan
509 et al. 2012).

510 Phosphate stripping was introduced 1991–1992 at the sewage treatment works at Tower
511 Wood (South Basin) and Ambleside (North Basin) (Fig. 11) and measured deep water
512 oxygen concentrations showed a marked improvement in the 1990s (Pickering, 2001). The
513 North Basin (SC68) shows a progressive decline in the $\delta^{15}N$ of organic matter indicating a
514 diminishing contribution from isotopically heavy sewage, which may in part be due to the
515 building of extra STW (sewage treatment works) at Gasmere and Elterwater (Fig. 11), but the
516 persistence of diatom ooze laminae resulting from diatom mass flux record sustained
517 eutrophication. On the other hand the $\delta^{15}N$ of organic matter in the South Basin (SC57)
518 shows no such decline, highlighting continued influence of isotopically heavy N in sewage
519 input. There is also a significant increase in organic carbon content in the North Basin.
520 Although phosphate stripping was introduced in 1991/ 1992, phosphate contents in the
521 sediment actually increase synchronously in all cores at this time and reach concentrations
522 of 1–2% in the surface sediment. Sustained concentrations of soluble reactive phosphorus are
523 also present in lake waters (Winfield et al., 2008). Microlithostratigraphic and EDS line scan
524 analysis show that P is associated with Fe oxyhydroxides in the top few cm of sediment,
525 suggesting redox mobilisation and potential P release from the sediment to lake waters (see
526 discussion on redox-driven processes in 4.2, above). This highlights the issue that although
527 external P loading may be reduced in mitigation programmes, internal P loading originating
528 by release from a pool earlier accumulated in the sediment may jeopardize improvement in
529 water quality (Søndergaard et al., 2003).

530 Since 1980, water column surveys identify both *Asterionella formosa* and *Aulacoseira* spp. to be
531 abundant in the spring (Canter and Haworth, 2010; Feuchtmayr et al., 2012; Haworth, 1988).
532 Other key spring bloom species present, include *Tabellaria flocculosa* and *Fragilaria crotonensis*

533 with *T. flocculosa* identified as more abundant than *Aulacoseira* spp. (Feuchtmayr et al., 2012).
534 These species do not form sediment laminae suggesting that they are less important for
535 controlling flux than either *Asterionella formosa* or *Aulacoseira subarctica*. The lamina records
536 show that *Aulacoseira subarctica* has replaced *Asterionella formosa* as the dominant lamina-
537 former since the early 1990s, matching with broader changes observed in the FBA plankton
538 records from the south end of the North Basin (Thackeray et al., 2015) (Fig. 12). Clearly, only
539 a few of the surface blooms recorded by the FBA correspond to laminae in SC68. This may
540 reflect some combination of the different locations (north end of the North Basin for the core
541 and south end for the FBA sampling), flux attenuation (so that only the most intense blooms
542 sedimented to depth) and intermittent bioturbation as evidenced by pelletisation (Fig. 3).
543 The installation of phosphate stripping to the Tower Wood STW in 1991/ 1992 has led to a
544 decrease in eutrophication. This is therefore consistent with the view that *Asterionella formosa*
545 favours fully eutrophic conditions while *Aulacoseira subarctica* thrives with moderate
546 increases in nutrients but is disadvantaged by further enrichment (Gibson et al., 2003).

547 Throughout Unit IV (1980 to the 2000's) the geochemistry and micropalaeontology of the
548 sediments show a partial recovery from eutrophication, but further indicate that the
549 recovery has not been sustained, consistent with evidence for a renewed deterioration in
550 oxygen levels in lake waters (Jones et al., 2008).

551 **4.4. The modern lake - 2010–2014: Topmost sediment and recent redox-driven**
552 **processes**

553 *4.4.1. Mn, Fe and Ba*

554 Microfabric and geochemical analysis shows that with the exception of SC67, the topmost
555 sediment of Unit I (1.5–3 cm) in all cores is enriched in Mn and Fe. This is consistent with
556 upwards diffusion of reduced and mobile Mn and Fe from the anoxic sediment and their

557 subsequent precipitation at the redox boundary near the SWI as oxyhydroxides (Davison,
558 1993). The exceptional concentrations of 12.5 wt% MnO in SC57 (Deep South Basin) requires
559 further explanation and suggests advection of Mn to the deep South Basin. The mechanism
560 for this may be analogous to that identified in the Swiss lake Baldaggersee where Mn
561 mobilisation leads to "geochemical focusing". This process involves the release of Mn from
562 anoxic sediments to overlying oxygenated waters where it starts to reprecipitate, but
563 because this take days to weeks there is down slope movement resulting in concentrations in
564 the deeper part of the lake (Schaller and Wehrli, 1997). A prerequisite for this to occur is for
565 anoxic sediment to be in contact with an oxic water column, a situation which is apparently
566 increasingly occurring during the stratified period in Windermere (Jones et al., 2008). A
567 similar redox-driven "geochemical focusing" process is also invoked for Fe, although this is
568 less mobile with a tendency to precipitate more rapidly as oxyhydroxides (Schaller and
569 Wehrli, 1997). The two cores that show the greatest Mn enrichment (SC 64 and SC57) also
570 show significant Ba enrichment to values exceeding 0.2 wt% in the deep South Basin. This
571 association is consistent with the sequestration of Ba by Mn oxyhydroxides (Section 4.3.3,
572 above) as also documented from Lake Biwa (Sugiyama et al., 1992).

573 *4.4.2. Arsenic*

574 There is relative enrichment of As in the surface sediments of SC68, SC64 and SC57 to values
575 approaching 70 ppm (Figs 3, 4). Arsenic is readily adsorbed by Fe oxyhydroxides in
576 sediment, and the cycles of Fe and As are tightly coupled (Belzile and Tessier, 1990; Couture
577 et al., 2010; Dixit and Hering, 2003; Pierce and Moore, 1982). Field and experimental
578 evidence indicates that As is also adsorbed by hydrous Mn oxide (Takamatsu et al., 1985)
579 and arsenite becomes adsorbed to more freshly formed Fe and Mn oxyhydroxides (Dixit and
580 Hering, 2003; Farmer and Lovell, 1986). This can lead to concentrations in surfaces
581 sediments far in excess of that delivered from the water column (Farmer and Lovell, 1986)

582 and has likely led to the enrichment of As in surface sediments of Windermere.
583 Furthermore, where a legacy of anthropogenic As pollution remains in deeper sediments, it
584 can remain elevated in the surface sediments long after exposure to anthropogenic sources
585 of As have been reduced (Fabian et al., 2003). There can be further enrichment of As in
586 surface sediments as a result of sediment anoxia where Fe and Mn oxyhydroxides and
587 adsorbed arsenate are reduced to labile species and diffuse upward to the redox boundary.
588 As is the case for Mn, As may be released to the water column during periods of lake
589 stratification, especially where hypoxia develops in the hypolimnion and remains for long
590 periods (Keimowitz et al., 2017). Progressive warming driven by climate change has
591 increased stratification in Windermere (Maberly and Elliott, 2012) so that this is likely to be
592 an ongoing process that may adversely affect the ecosystems (Thackeray et al., 2013)
593 including fisheries (Jones et al., 2008).

594 **4.5. Implications for future water quality and potential hazards**

595 Many countries, including the UK, have failed to introduce the formal Sediment Quality
596 Standards (SQS) such as those set by the Australian, New Zealand (ANZECC/ARMCANZ,
597 2000), Canadian (CCME EPC-98E), and Netherlands governments (Dutch Water Act) (Fig.
598 14) (Burton Jr, 2002). These are designed to be adopted to control sediment contamination
599 considered dangerous to benthic life and human health (Burton Jr, 2002). The enrichment of
600 Pb and As in Unit III (especially in the 20th century) too often exceed these standards in both
601 of the South Basin cores for Pb. Concentrations of As in all cores, (except SC64) also exceed
602 the exceed the SQS (Fig. 14). This is concerning if these sediments were to be exposed to
603 water column hypoxic or disoxia conditions where both Pb and As can become mobile
604 (Hamilton-Taylor and Davison, 1995). Evidence of mass transport deposits and slope failure
605 scarps found in the distal lake slopes suggest that this is increasingly possible (Fielding et
606 al., 2018; Miller et al., 2013). What is more concerning is that in both North Basin cores, As

607 values at the SWI exceed all three SQS. As discussed, Mn and As dissolution and migration
608 under low oxygen conditions to the above water column is common in warm monomictic
609 lakes during the Summer/ Autumn bottom water oxygen low (Keimowitz et al., 2017). This
610 would suggest that significant quantities of As are mobile and being released into the water
611 column during Summer and Autumn months (El Bilali et al., 2002). As discussed above the
612 Water Framework Directive legally obliges stakeholders to return water bodies to "good
613 ecological and chemical status" with reference to pre-anthropogenic chemical, ecological
614 and environmental conditions. Our combined geochemical and sediment microfabric study
615 demonstrates that, despite mitigation measures being put in place, pollution issues still
616 remain in Windermere. With climate change driving current trends of longer and more
617 intense summer lake stratification, the degree of mobilisation of toxic elements may increase
618 in the future, requiring a reappraisal of mitigation strategies.

619

620 ## 5. Conclusions

621 A multi-proxy investigation of sediment cores from Windermere, England's largest natural
622 lake, has yielded a detailed history of changing lake and catchment conditions over the past
623 300 years. Prior to the 19th century in the lake's South Basin and the 20th century in the North
624 Basin, Fe and Mn rich laminae indicate regular, seasonal-scale ventilation of bottom waters.
625 Following local population increases and associated increasing fossil fuel use through the
626 19th century, Pb content in the sediment increases first in the South Basin (SC67–1810s; SC57–
627 1850s) and from 1910–20 in the North Basin. This is followed later by increases in other
628 metals (Zn, Cu, Hg), and As. At the same time increases in sedimentary $\delta^{13}C$, and the
629 appearances of monospecific diatom ooze lamina, together with decreasing Fe and Mn
630 lamina show a move to decreasing bottom water ventilation caused by eutrophication.

Greater values of sedimentary $\delta^{15}N$ through the same period are also consistent with enhanced productivity coupled with increases in sewage discharge and farm runoff in to the lake, with the latter two inputs being likely sources of metals and nutrient enrichment. The synchronous increase in metals with indicators of lake productivity also point toward the enhanced incorporation and adsorption of metals to settling diatom aggregates bringing elevated flux to the sediments. Through the middle of the 20th century benthic activity intermittently ceased in the deeper North Basin due to persistent strongly reducing conditions in the sediment and bottom waters as indicated by increased S content, low Fe–Mn values and the formation of unusual Pb-bearing barite mineralisation, hitherto only described from toxic mine wastes and contaminated soils. From 1980 there was a partial recovery, with bioturbated sediment reflecting increases in oxygenation of deep waters. In the South Basin however, elevated $\delta^{15}N$ of organic matter indicates continued impacts of sewage discharge. Imaging and X-ray microanalysis using scanning electron microscopy has enabled the identification of seasonal-scale redox mineralisation of Mn, Fe, Ba related to intermittent sediment anoxia. Recent, persistent sediment anoxia, strengthened by hypoxic bottom waters during seasonal stratification, has resulted in trace element mobilisation. Subsequent oxidation at the SWI or within the bottom waters has caused significant enrichment of Mn, Fe, As, P and Ba in the surficial sediment, and in the North Basin, As enrichment at the surface exceeds Sediment Quality Standards set by the Australian, New Zealand, Canadian and Netherlands governments. It would thus appear that despite mitigation measures being put in place pollution issues still remain in Windermere, and with climate change driving current trends of increased duration of summer stratification in the lake, the mobilisation of toxic elements may increase in the future.

Acknowledgements: In addition to those mentioned in the funding acknowledgments the authors would like to express their gratitude to the Rock Preparation and Thin-Sectioning Laboratory and the Stable Isotope Mass-spectrometry at the National Oceanography Centre,

UK. We would also like to thank Kate Davis for her assistance with drafting some figures. Finally, we would like to thank the reviewers whose helpful comments improved this manuscript greatly. This work was supported by the NERC Radiocarbon Facility NRCF010001 (allocation numbers 1856.1014 and 1736.1013). This research was supported by a University of Southampton Studentship Grant and a Natural Environmental ResearchCouncil Studentship Grant (NE/L50161X/1).

References

Avery RS, Xuan C, Kemp AE, Bull JM, Cotterill CJ, Fielding JJ, et al. A new Holocene record of geomagnetic secular variation from Windermere, UK. Earth and Planetary Science Letters 2017; 477: 108–122.

Belzile N, Tessier A. Interactions between arsenic and iron oxyhydroxides in lacustrine sediments. Geochimica et Cosmochimica Acta 1990; 54: 103–109.

Bhaskar P, Bhosle NB. Bacterial extracellular polymeric substance (EPS): a carrier of heavy metals in the marine food-chain. Environment International 2006; 32: 191–198.

Brodersen KP. SJ Brooks, PG Langdon and O. Heiri, The Identification and Use of Palaearctic Chironomidae Larvae in Palaeoecology. QRA Technical Guide No. 10. Springer, 2008.

Burton Jr GA. Sediment quality criteria in use around the world. Limnology 2002; 3: 65-76.

Canter HM, Haworth EY. The occurrence of two new plankton diatom populations in the English Lake District: *Aulacoseira islandica*. Freshwater Forum. 1, 2010.

Carvalho L, Mackay EB, Cardoso AC, Baattrup-Pedersen A, Birk S, Blackstock KL, Borics G, Borja A, Feld CK, Ferreira MT, Globevnik L. Protecting and restoring Europe's waters: an analysis of the future development needs of the Water Framework Directive. Science of the Total Environment. 2019 Mar 25;658:1228-38.

Comte S, Guibaud G, Baudu M. Biosorption properties of extracellular polymeric substances (EPS) towards Cd, Cu and Pb for different pH values. Journal of hazardous materials 2008; 151: 185-193.

Courtin-Nomade A, Soubrand-Colin M, Marcus MA, Fakra SC. Evidence for the incorporation of lead into barite from waste rock pile materials. Environmental Science & Technology 2008; 42: 2867-2872.

Couture R-M, Gobeil C, Tessier A. Arsenic, iron and sulfur co-diagenesis in lake sediments. Geochimica et Cosmochimica Acta 2010; 74: 1238-1255.

Croudace IW, Rindby A, Rothwell RG. ITRAX: description and evaluation of a new multi-function X-ray core scanner. Geological Society, London, Special Publications 2006; 267: 51-63.

Croudace IW, Warwick PE, Morris JE. Evidence for the preservation of technogenic tritiated organic compounds in an estuarine sedimentary environment. Environmental Science and Technology 2012; 46: 5704-5712.

Damon PE, Donahue D, Gore B, Hatheway A, Jull AT, Linick T, et al. Radiocarbon dating of the Shroud of Turin. Nature 1989; 337: 611-615.

Davison W. Iron and manganese in lakes. Earth-Science Reviews 1993; 34: 119-163.

699 Davison W, Lishman J, Hilton J. Formation of pyrite in freshwater sediments: Implications
700 for C/S ratios. Geochimica et Cosmochimica Acta 1985; 49: 1615-1620.
701 Dean JM, Kemp AES, Bull D, Pike J, Patterson G, Zolitschka B. Taking varves to bits:
702 Scanning electron microscopy in the study of laminated sediments and varves.
703 Journal of Paleolimnology 1999; 22: 121-136.
704 Dixit S, Hering JG. Comparison of arsenic (V) and arsenic (III) sorption onto iron oxide
705 minerals: implications for arsenic mobility. Environmental Science and Technology
706 2003; 37: 4182-4189.
707 Dudgeon D, Arthington AH, Gessner MO, Kawabata Z-I, Knowler DJ, Lévêque C, et al.
708 Freshwater biodiversity: importance, threats, status and conservation challenges.
709 Biological Reviews 2006; 81: 163-182.
710 El Bilali L, Rasmussen P, Hall G, Fortin D. Role of sediment composition in trace metal
711 distribution in lake sediments. Applied Geochemistry 2002; 17: 1171-1181.
712 Fabian D, Zhou Z, Wehrli B, Friedl G. Diagenetic cycling of arsenic in the sediments of
713 eutrophic Baldeggersee, Switzerland. Applied Geochemistry 2003; 18: 1497-1506.
714 Fakhraee M, Li J, Katsev S. Significant role of organic sulfur in supporting sedimentary
715 sulfate reduction in low-sulfate environments. Geochimica et Cosmochimica Acta
716 2017; 213: 502-516.
717 Famme P, Knudsen J. Anoxic survival, growth and reproduction by the freshwater annelid,
718 Tubifex sp., demonstrated using a new simple anoxic chemostat. Comparative
719 Biochemistry and Physiology Part A: Physiology 1985; 81: 251-253.
720 Farmer J, Lovell M. Natural enrichment of arsenic in Loch Lomond sediments. Geochimica
721 et Cosmochimica Acta 1986; 50: 2059-2067.
722 Fernandez-Gonzalez A, Carneiro J, Katsikopoulos D, Prieto M. Thermodynamic properties
723 of the (Ba,Pb)SO4 solid solution under ambient conditions: Implications for the
724 behavior of Pb and Ra in the environment. Geochimica et Cosmochimica Acta 2013;
725 105: 31-43.
726 Feuchtmayr H, Thackeray SJ, Jones ID, De Ville M, Fletcher J, James B, et al. Spring
727 phytoplankton phenology - are patterns and drivers of change consistent among
728 lakes in the same climatological region? Freshwater Biology 2012; 57: 331-344.
729 Fielding JJ, Kemp AES, Bull JM, Cotterill CJ, Pearce RB, Avery RS, et al. Palaeoseismology
730 from microfabric and geochemical analysis of lacustrine sediments, Windermere,
731 UK. Journal of the Geological Society 2018; 175: 903-914.
732 Finlay BJ, Hetherington NB, Davison W. Active Biological Participation in Lacustrine
733 Barium Chemistry. Geochimica et Cosmochimica Acta 1983; 47: 1325-1329.
734 Flynn W. The determination of low levels of polonium-210 in environmental materials.
735 Analytica Chimica Acta 1968; 43: 221-227.
736 Förstner U, Wittmann GT. Metal pollution in the aquatic environment: Springer Science &
737 Business Media, 2012.
738 Fowler H, Kilsby C, Stunell J. Modelling the impacts of projected future climate change on
739 water resources in north-west England. Hydrology and Earth System Sciences
740 Discussions 2007; 11: 1115-1126.
741 Gibson CE, Anderson NJ, Haworth EY. *Aulacoseira subarctica*: taxonomy, physiology, ecology
742 and palaeoecology. European Journal of Phycology 2003; 38: 83-101.
743 Goldstein JI, Newbury DE, Echlin P, Joy DC, Lyman CE, Lifshin E, et al. Quantitative X-ray
744 analysis: the basics. Scanning Electron Microscopy and X-ray Microanalysis.
745 Springer, 2003, pp. 391-451.
746 Gu, B., Alexander, V. and Schell, D.M., Seasonal and interannual variability of plankton
747 carbon isotope ratios in a subarctic lake. Freshwater Biology 1999; 42(3): 417-426.

748 Gulati, R.D., Pires, L.M.D., Van Donk, E., 2012. Restoration of freshwater lakes, in: van
749 Andel, J., Aronson, J. (Eds.), Restoration Ecology: The New Frontier. Blackwells,
750 London, pp. 233-247.
751 Hamilton-Taylor J, Willis M. A quantitative assessment of the sources and general dynamics
752 of trace metals in a soft-water lake. Limnology and Oceanography 1990; 35: 840-851.
753 Hamilton-Taylor J. Enrichments of zinc, lead, and copper in recent sediments of
754 Windermere, England. Environmental Science & Technology 1979; 13: 693-697.
755 Hamilton-Taylor J, Davison W. Redox-driven cycling of trace elements in lakes. Physics and
756 chemistry of lakes. Springer, 1995, pp. 217-263.
757 Hamilton-Taylor J, Willis M, Reynolds C. Depositional fluxes of metals and phytoplankton
758 in Windermere as measured by sediment traps. Limnology and Oceanography 1984;
759 29: 695-710.
760 Harvey D, Thompson N, Charles S, Hubbard C. Farming and Farm Forestry in the Lake
761 District: A report for the Lake District National Park Partnership Farming and
762 Forestry Task Force. 1. Centre for Rural Economy, Newcastle University, 2012.
763 Haworth E. Distribution of diatom taxa of the old genus Melosira (now mainly *Aulacoseira*)
764 in Cumbrian waters. In: F E Round (Ed) Algae and the Aquatic Environment, Bristol
765 Biopress 1988: 138-167.
766 Hodell DA, Schelske CL. Production, sedimentation, and isotopic composition of organic
767 matter in Lake Ontario. Limnology and Oceanography 1998; 43: 200-214.
768 Hutchinson, G.E. and Löffler, H., 1956. The thermal classification of lakes. Proceedings of the
769 National Academy of Sciences of the United States of America, 42(2), p.84.
770 Itai T, Hayase D, Hyobu Y, Hirata SH, Kumagai M, Tanabe S. Hypoxia-induced exposure of
771 isaza fish to manganese and arsenic at the bottom of Lake Biwa, Japan: experimental
772 and geochemical verification. Environmental science & technology. 2012 Jun
773 5;46(11):5789-97.
774 Jenny JP, Arnaud F, Alric B, Dorioz JM, Sabatier P, Meybeck M, Perga ME. Inherited
775 hypoxia: A new challenge for reoligotrophicated lakes under global warming. Global
776 Biogeochemical Cycles. 2014 Dec 1;28(12):1413-23.
777 Jones ID, Winfield IJ, Carse F. Assessment of long-term changes in habitat availability for
778 Arctic charr (Salvelinus alpinus) in a temperate lake using oxygen profiles and
779 hydroacoustic surveys. Freshwater Biology 2008; 53: 393-402.
780 Keimowitz AR, Mailloux BJ, Wovkulich K, Harkness JS, Ross JM, Chillrud SN. Manganese
781 redox buffering limits arsenic release from contaminated sediments, Union Lake,
782 New Jersey. Applied geochemistry 2017; 77: 24-30.

783 Kemp AES, Dean J, Pearce RB, Pike J. Recognition and analysis of bedding and sediment
784 fabric features. In: Last WM, Smol JP, editors. Tracking Environmental Change Using
785 Lake Sediments. Volume 2: Physical and Geochemical Methods. Kluwer Academic
786 Publishers, Dordrecht, 2001, pp. 7-22.
787 Lehmann MF, Bernasconi SM, Barbieri A, McKenzie JA. Preservation of organic matter and
788 alteration of its carbon and nitrogen isotope composition during simulated and in
789 situ early sedimentary diagenesis. Geochimica et Cosmochimica Acta 2002; 66: 3573-
790 3584.

791 Lund J. Chemical analysis in ecology illustrated from Lake District tarns and lakes. 2. Algal
792 differences. Proceedings of the Linnean Society of London. 167. Wiley Online
793 Library, 1957, pp. 165-171.
794 Lund JWG. Eutrophication. Proceedings of the Royal Society of London. Series B. Biological
795 Sciences 1972; 180: 371-382.

796 Lund JWG, Mackereth FJH, Mortimer CH. Changes in depth and time of certain chemical
797 and physical conditions and of the standing crop of *Asterionella formosa* Hass. in the
798 North Basin of Windermere in 1947. Philosophical Transactions of the Royal Society
799 of London. Series B, Biological Sciences 1963; 246: 255-290.
800 Maberly S, De Ville M, Thackeray S, Feuchtmayr H, Fletcher J, James J, et al. A survey of the
801 lakes of the English Lake District: The Lakes Tour 2010. 2011. NERC/Centre for
802 Ecology & Hydrology.
803 Maberly S, Elliott J. Insights from long-term studies in the Windermere catchment: external
804 stressors, internal interactions and the structure and function of lake ecosystems.
805 Freshwater Biology 2012; 57: 233-243.
806 Maltby E, Ormerod S, Acreman M, Dunbar M, Jenkins A, Maberly S, et al. Freshwaters:
807 openwaters, wetlands and floodplains [chapter 9]. 2011.
808 McCall PL, Tevesz MJ. The effects of benthos on physical properties of freshwater
809 sediments. Animal-Sediment Relations. Springer, 1982, pp. 105-176.
810 McGowan S, Barker P, Haworth EY, Leavitt PR, Maberly SC, Pates J. Humans and climate as
811 drivers of algal community change in Windermere since 1850. Freshwater Biology
812 2012; 57: 260-277.
813 Meyers PA. Preservation of elemental and isotopic source identification of sedimentary
814 organic matter. Chemical Geology 1994; 114: 289-302.
815 Miller H, Bull JM, Cotterill CJ, Dix JK, Winfield IJ, Kemp AE, et al. Lake bed geomorphology
816 and sedimentary processes in glacial lake Windermere, UK. Journal of Maps 2013; 9:
817 299-312.
818 Miller H, Croudace IW, Bull JM, Cotterill CJ, Dix JK, Taylor RN. A 500 year sediment lake
819 record of anthropogenic and natural inputs to Windermere (English Lake District)
820 using double-spike lead isotopes, radiochronology, and sediment microanalysis.
821 Environmental Science and Technology 2014; 48: 7254-7263.
822 Miller H, Winfield IJ, Fletcher JM, Ben James J, Rijn J, Bull JM, et al. Distribution,
823 characteristics and condition of Arctic charr (Salvelinus alpinus) spawning grounds
824 in a differentially eutrophicated twin-basin lake. Ecology of Freshwater Fish 2015; 24:
825 32-43.
826 Moorhouse, H.L., McGowan, S., Jones, M.D., Barker, P., Leavitt, P.R., Brayshaw, S.A.,
827 Haworth, E.Y., 2014. Contrasting effects of nutrients and climate on algal
828 communities in two lakes in the Windermere catchment since the late 19th century.
829 Freshwater Biology 59, 2605-2620.
830 Moorhouse HL, McGowan S, Taranu ZE, Gregory-Eaves I, Leavitt PR, Jones MD, Barker P,
831 Brayshaw SA. Regional versus local drivers of water quality in the Windermere
832 catchment, Lake District, United Kingdom: The dominant influence of wastewater
833 pollution over the past 200 years. Global change biology. 2018 Sep;24(9):4009-22.
834 Musson R, Henni P. The felt effects of the Carlisle earthquake of 26 December 1979. Scottish
835 Journal of Geology 2002; 38: 113-125.
836 Naeher S, Gilli A, North RP, Hamann Y, Schubert CJ. Tracing bottom water oxygenation
837 with sedimentary Mn/Fe ratios in Lake Zurich, Switzerland. Chemical Geology 2013;
838 352: 125-133.
839 Och LM, Müller B, Voegelin A, Ulrich A, Göttlicher J, Steiniger R, et al. New insights into the
840 formation and burial of Fe/Mn accumulations in Lake Baikal sediments. Chemical
841 Geology 2012; 330: 244-259.
842 Ochsenbein U, Davison W, Hilton J, Haworth E. The Geochemical Record of Major Cations
843 and Trace Metals in a Productive Lake; Analysis of Thinly Sliced Sediment Samples
844 Characterised by Diatom Stratigraphy. Archiv fur Hydrobiologie 1983; 98.
845 Pearsall WH, Pennington W. The Lake District: a landscape history. London: Collins 320p.-
846 Illus., maps.. Geog 1973; 1.

847 Pennington W. The recent sediments of Windermere. Freshwater Biology 1973; 3: 363-382.
848 Pickering AD, Sutcliffe DW. Windermere: restoring the health of England's largest lake:
849 Freshwater Biological Association, 2001.
850 Pierce ML, Moore CB. Adsorption of arsenite and arsenate on amorphous iron hydroxide.
851 Water Research 1982; 16: 1247-1253.
852 Pretty JN, Mason CF, Nedwell DB, Hine RE, Leaf S, Dils R. Environmental costs of
853 freshwater eutrophication in England and Wales. ACS Publications, 2003.
854 Reimer PJ, Bard E, Bayliss A, Beck JW, Blackwell PG, Ramsey CB, et al. IntCal13 and
855 Marine13 radiocarbon age calibration curves 0–50,000 years cal BP. Radiocarbon
856 2013; 55: 1869-1887.
857 Reynolds G, Hamilton-Taylor J. The role of planktonic algae in the cycling of Zn and Cu in a
858 productive soft-water lake. Limnology and Oceanography 1992; 37: 1759-1769.
859 Reynoldson TB. The role of environmental factors in the ecology of tubificid oligochaetes-an
860 experimental study. Ecography 1987; 10: 241-248.
861 Richardson K, Jørgensen BB. Eutrophication: definition, history and effects. Eutrophication
862 in coastal marine ecosystems 1996: 1-19.
863 Rippey B, Douglas RW. Reconstructing regional-scale lead contamination of the atmosphere
864 (1850–1980) in the United Kingdom and Ireland using lake sediments. Global
865 Biogeochemical Cycles 2004; 18.
866 Ritchie JC, McHenry JR. Application of radioactive fallout cesium-137 for measuring soil
867 erosion and sediment accumulation rates and patterns: a review. Journal of
868 Environmental Quality 1990; 19: 215-233.
869 Robbins JA. Geochemical and geophysical applications of radioactive lead isotopes. In:
870 Nriagu JO, editor. Biochemistry of Lead. Elsevier, Amsterdam, 1978, pp. 285-393.
871 Sabater S, Haworth EY. An assessment of recent trophic changes in Windermere South Basin
872 (England) based on diatom remains and fossil pigments. Journal of Paleolimnology
873 1995; 14: 151-163.
874 Schaller T, Moor HC, Wehrli B. Sedimentary profiles of Fe, Mn, V, Cr, As and Mo as
875 indicators of benthic redox conditions in Baldeggersee. Aquatic sciences 1997; 59:
876 345-361.
877 Schaller T, Wehrli B. Geochemical-focusing of manganese in lake sediments—an indicator of
878 deep-water oxygen conditions. Aquatic Geochemistry 1996; 2: 359-378.
879 Schelske CL, Hodell DA. Using carbon isotopes of bulk sedimentary organic matter to
880 reconstruct the history of nutrient loading and eutrophication in Lake Erie.
881 Limnology and Oceanography 1995; 40: 918-929.
882 Schillereff DN, Chiverrell RC, Macdonald N, Hooke JM, Welsh KE, Piliposian G, Croudace
883 IW. Convergent human and climate forcing of late-Holocene flooding in Northwest
884 England. Global and Planetary Change. 2019 Nov 1;182:102998.
885 Schweitzer B, Huber I, Amann R, Ludwig W, Simon M. α-and β-Proteobacteria control the
886 consumption and release of amino acids on lake snow aggregates. Applied and
887 Environmental Microbiology 2001; 67: 632-645.
888 Smith E, Hamilton-Taylor J, Davison W, Fullwood NJ, McGrath M. The effect of humic
889 substances on barite precipitation-dissolution behaviour in natural and synthetic lake
890 waters. Chemical Geology 2004; 207: 81-89.
891 Søndergaard M, Jensen JP, Jeppesen E. Role of sediment and internal loading of phosphorus
892 in shallow lakes. Hydrobiologia. 2003 Nov 1;506(1-3):135-45.
893 Spears B. M., UK Centre for Ecology and Hydrology, 2014. UK lake restoration.
894 https://www.ceh.ac.uk/our-science/projects/uk-lake-restoration (accessed 03
895 February, 2020).
896 Stuiver M, Reimer PJ. Extended ^{14}C data base and revised CALIB 3.0 ^{14}C age calibration
897 program. Radiocarbon 1993; 35: 215-230.

Sugiyama M, Hori T, Kihara S, Matsui M. A geochemical study on the specific distribution of barium in Lake Biwa, Japan. Geochimica et Cosmochimica Acta 1992; 56: 597-605.
Takamatsu T, Kawashima M, Koyama M. The role of Mn2+-rich hydrous manganese oxide in the accumulation of arsenic in lake sediments. Water Research 1985; 19: 1029-1032.
Talling J, Heaney S. Long-term changes in some English (Cumbrian) lakes subjected to increased nutrient inputs. In: F E Round (Ed) Algae and the Aquatic Environment, Bristol Biopress 1988: 1-29.
Thackeray, S.J.; De Ville, M.M.; Fletcher, J.M.; James, J.B.; Maberly, S.C.; Mackay, E.B.; Winfield, I.J. Cumbrian Lakes plankton and fish data (1940 to 2013). NERC Environmental Information Data Centre 2015.
Thackeray SJ, Henrys PA, Feuchtmayr H, Jones ID, Maberly SC, Winfield IJ. Food web de-synchronization in E ngland's largest lake: an assessment based on multiple phenological metrics. Global Change Biology 2013; 19: 3568-3580.Thampapillai DJ, Musgrave WF. Flood damage mitigation: A review of structural and nonstructural measures and alternative decision frameworks. Water Resources Research 1985; 21: 411-424.
Thevenon F, Graham ND, Chiaradia M, Arpagaus P, Wildi W, Poté J. Local to regional scale industrial heavy metal pollution recorded in sediments of large freshwater lakes in central Europe (lakes Geneva and Lucerne) over the last centuries. Science of the Total Environment 2011; 412: 239-247.
Williamson CE, Saros JE, Vincent WF, Smol JP. Lakes and reservoirs as sentinels, integrators, and regulators of climate change. Limnology and Oceanography 2009; 54: 2273-2282.
Winfield IJ, Fletcher JM, James JB. The Arctic charr (Salvelinus alpinus) populations of Windermere, UK: population trends associated with eutrophication, climate change and increased abundance of roach (Rutilus rutilus). Environmental Biology of Fishes. 2008 Sep 1;83(1):25-35.
Woolway RI, Simpson JH, Spiby D, Feuchtmayr H, Powell B, Maberly SC. Physical and chemical impacts of a major storm on a temperate lake: a taste of things to come?. Climatic change. 2018 1;151(2):333-47.
Wu Q, Qi J, Xia X. Long-term variations in sediment heavy metals of a reservoir with changing trophic states: Implications for the impact of climate change. Science of the Total Environment. 2017 Dec 31;609:242-50.
Xue H, Gächter R, Sigg L. Comparison of Cu and Zn cycling in eutrophic lakes with oxic and anoxic hypolimnion. Aquatic Sciences 1997; 59: 176-189.
Yu C, Virtasalo JJ, Österholm P, Burton ED, Peltola P, Ojala AE, et al. Manganese accumulation and solid-phase speciation in a 3.5 m thick mud sequence from the estuary of an acidic and Mn-rich creek, northern Baltic Sea. Chemical Geology 2016; 437: 56-66.
Zolitschka B, Francus P, Ojala AE, Schimmelmann A. Varves in lake sediments–a review. Quaternary Science Reviews 2015; 117: 1-41.

Figure and table captions

Fig. 1. Location of study area and cores. Inset shows position of Windermere in relation to the Lake District topography. The extent of the Windermere catchment is given by the

dashed line. Key rivers and water bodies feeding the lake are shown, together with major population centres and sewage treatment works (Triangles). *(1.5 column fitting image)*

Fig. 2. Age depth model measurements of artificial radionuclides for cores SC68 (a), SC64 (b), SC67 (c), SC57 (d) and calculated linear sedimentation rates (LSR). R^2 shows the linear trend for the Ln ^{210}Pbxs data. In the age panel black circles show the ^{210}Pb CF:CS LSR age depth model at 2 cm intervals. Vertical error indicates bulk sample interval and horizontal error represents the extent of the maximum and minimum age depth based on machine measurement error. White circles show the ^{137}Cs based age depth at 1986 and 1963 with vertical error also indicating the bulk sample interval. Red circles show data points that were removed due to being partly within the mass transport deposit (MTD). Grey triangles show the age depth at the base of the core derived from linear interpilation between ^{210}Pb and ^{14}C derived ages (Table 2)*(2 column fitting image).*

Fig. 3. Stratigraphy and Geochemistry for North Basin Cores SC68 and SC64. Core depth in cm, core photograph, core x-radiograph, lithological units, lithostratigraphy, sediment fabric types, ^{210}Pb CF:CS LSR age depth model for the North Basin gravity cores. For geochemistry black lines show Itrax ED-XRF Fe, Mn, Pb, As, S and P (lower scale). Red dots show discreet WD-XRF data for K_2O, Fe_2O_3, MnO, Pb, As, S and P_2O_5 (titles in brackets, upper scales). Vertical errors on WD-XRF show the sampling interval. Water depths of each coring site are shown above the corresponding core. *(2 column fitting image).*

Fig. 4. Stratigraphy and Geochemistry for South Basin Cores SC67 and SC57. Core depth in cm, core photograph, core x-radiograph, lithological units, lithostratigraphy, sediment fabric types, ^{210}Pb CF:CS LSR age depth model for the South Basin gravity cores. For geochemistry black lines show Itrax ED-XRF Fe, Mn, Pb, As, S and P (lower scale). Red dots show discreet WD-XRF data for K_2O, Fe_2O_3, MnO, Pb, As, S and P_2O_5 (titles in brackets, upper scales).

966 Vertical errors on WD-XRF show the sampling interval. Water depths of each coring site are
967 shown above the corresponding core. *(2 column fitting image).*

968 **Fig. 5**. Organic chemistry for SC68 and SC57. Core depth in cm, core photograph, core x-
969 radiograph, lithostratigraphy, sediment fabric types, ^{210}Pb CF:CS LSR age depth model for
970 the South Basin gravity cores. This is followed by $\delta^{13}C$, $\delta^{15}N$, TOC, TN, C/N (grey dots).
971 Vertical error shows the sampling interval for each data point *(2 column fitting image)*.

972 **Fig. 6**. Detailed sediment and microfabric types as identified using optical thin section
973 microscopy (left) and backscatter electron imagery (middle). Fabric types: [a] pelleted [b]
974 homogenous, [c] laminated (alternating porous and terrigenous-rich laminae), [d] dark
975 muds. Key sediment fabric features are featured (left). *(1.5 column fitting image).*

976 **Fig. 7.** Position of *Aulacoseira subarctica* bloom lamina (A) within SC11 optical thin section
977 and back scatter electron image (BSEI) and *Asterionella formosa* bloom lamina (B) within SC14
978 optical thin section and BSEI, and detailed optical thin section and BSEI form both A and B.
979 *(2 column fitting image).*

980 **Fig. 8.** Core photograph of SC68 with depth and age showing the position of rhodochrosite
981 minerals shown in panel A, with corresponding EDS elemental map showing Mn
982 highlighted in purple. Lower panel shows the EDS line scan of Mn and Ca in mineral across
983 x–y. Panel B shows amorphous Fe oxyhydroxide, as determined by EDS from location
984 indicated in panel A. *(2 column fitting image).*

985 **Fig. 9.** Optical thin section, back scatter electron image, mineral lamina log, EDS map (Si, Mn
986 and Fe) and EDS line scan (Si, Mn and Fe) of alternating laminae for thin sections (A)
987 SC68_19, (B) SC68_20 and (C) SC68_21 from SC68. *(2 column fitting image). (2 column fitting*
988 *image).*

989 **Fig. 10.** Core SC68 photograph along with depth and age showing the position of samples
990 containing examples of (A) multiple barite-anglesite minerals, and (B, top) and individual
991 barite-anglesite mineral. (B, bottom) Also shown is an EDS line scan of Pb, Ba and S in
992 mineral B. *(2 column fitting image).*

993 **Fig. 11.** A time line of the anthropogenic environmental variables. Modern artificial fertiliser
994 manufacturing began in the UK in the early 20th century (dashed line), exceeded 200 Tonnes
995 (N x 10^{3}) use nationwide in ~1945 (solid line) and peaked in ~1990 (diamond) (McGowan et
996 al. 2012). Δ15N and aspects of significant sediment chemistry results from this paper are
997 shown for the North (SC68) and South Basin (SC57). For chemistry, solid lines represent
998 onset and increase in concentration; dashed lines represent decreasing values. Full
999 geochemistry is given in Figs 3 and 4 and discussed in the text. *(1.5 column fitting image).*

1000 **Fig. 12.** Comparison of sediment diatom record with FBA diatom record through the period
1001 1977–2014. Asta - *Asterionella Formosa*; Aula - *Aulacoseira subarctica*. *(1 column fitting image)*

1002 **Fig. 13.** SC68 (a), SC64 (b), SC67 (c) and SC57 (d) Pb (black dots, left y-axis), As (red
1003 triangles, right y-axis) concentrations over time along with Australian-New Zealand,
1004 Canadian (short dashes) and Netherlands (long dashes) sediment quality standards for Pb
1005 (black) and As (red). *(2 column fitting image)*

1006 **Table 1**. Gravity core location description and coordinates, depth and length.

1007 **Table 2**. The depth, age and 2σ calibrated ages of the top most ^{14}C from the piston cores at
1008 each site. The depth scale is composite constructed using overlap between the gravity and
1009 piston cores. Mean ages and radiocarbon 2σ age ranges are expressed years before present
1010 (1950 A.D.).
1011

1012 Figure 1

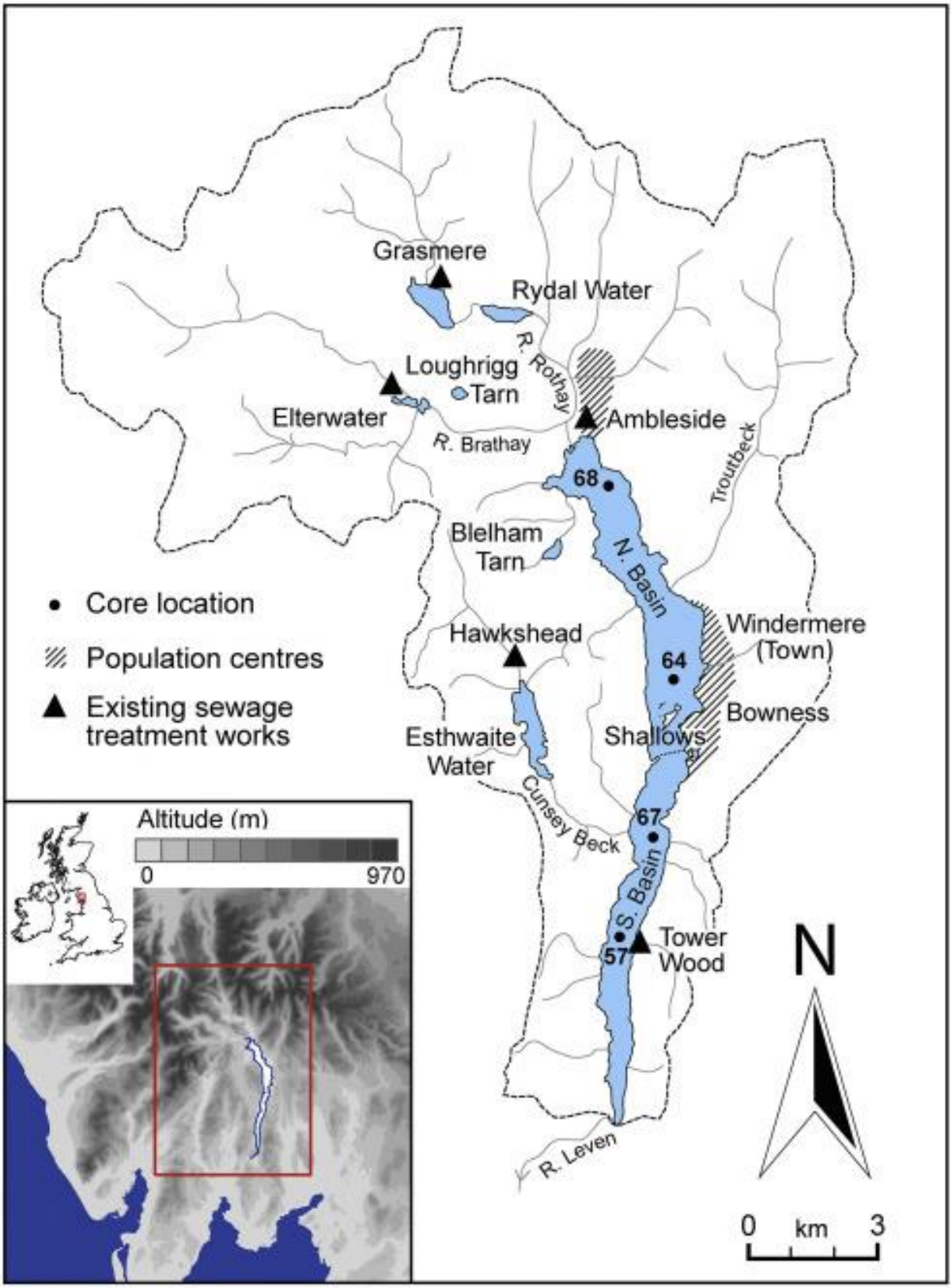

1013

1014

1015 Figure 2

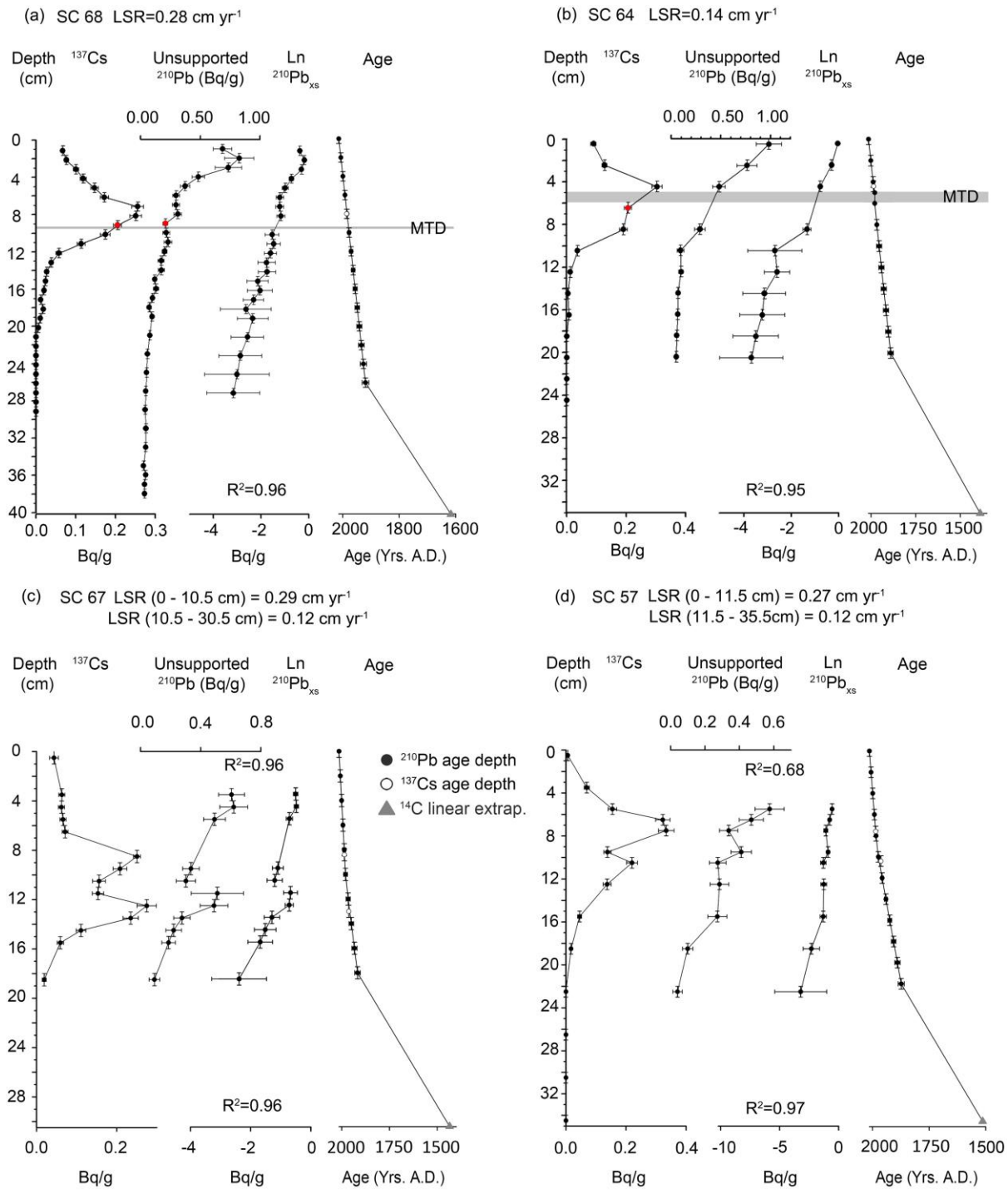

1016

1017

1018 Figure 3

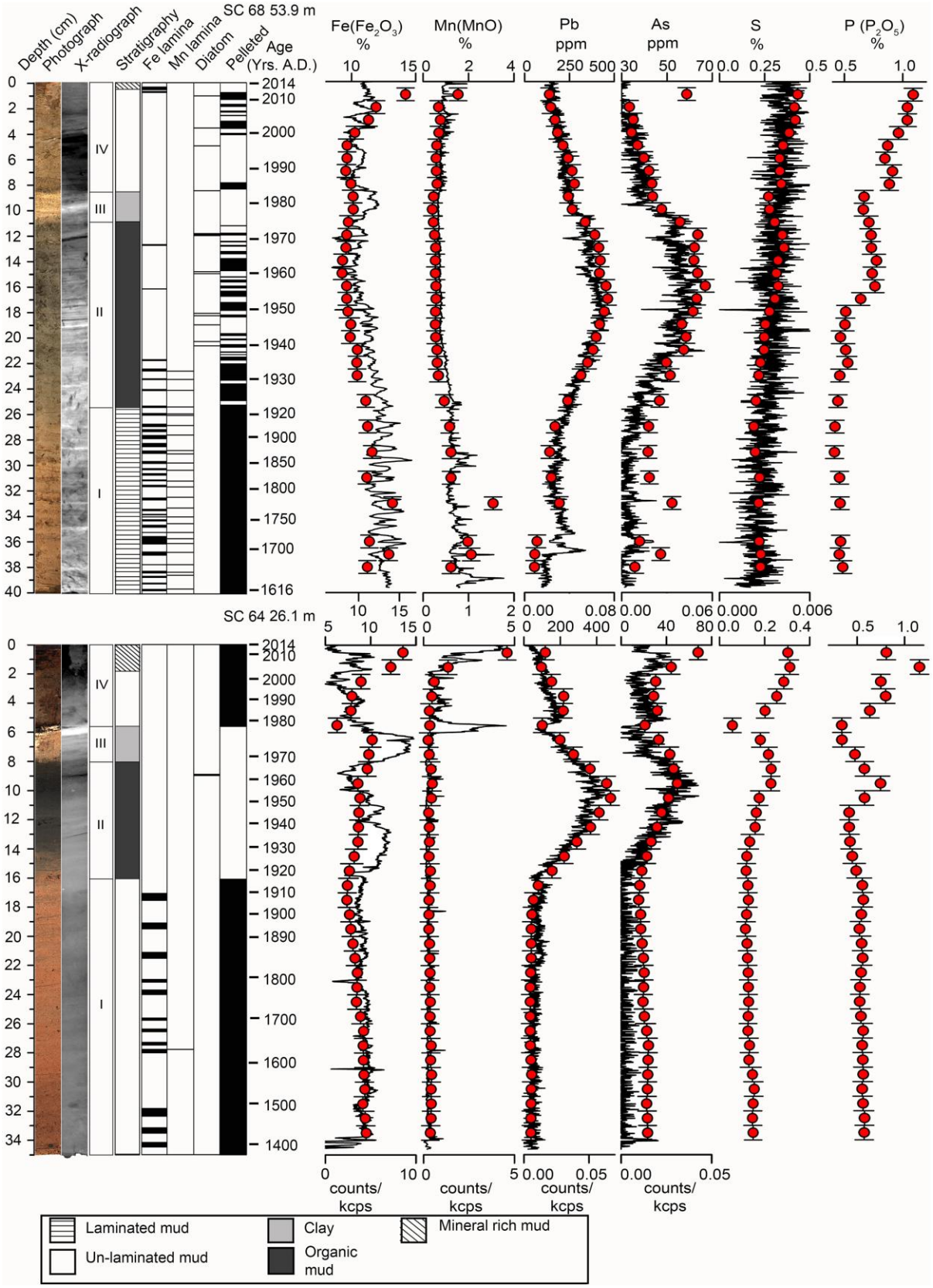

1019

1020

1021 Figure 4

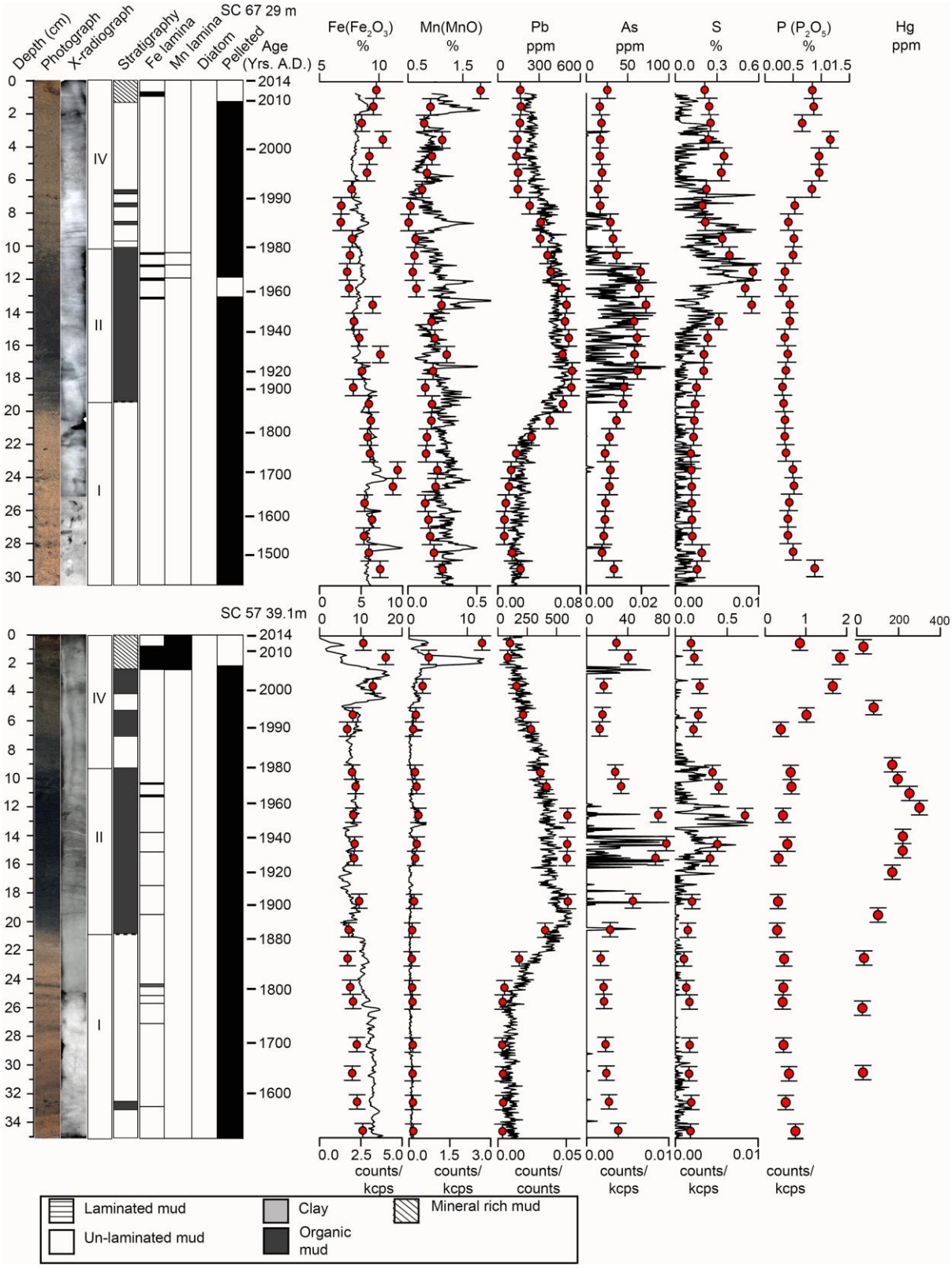

1022

1023

1024 Figure 5

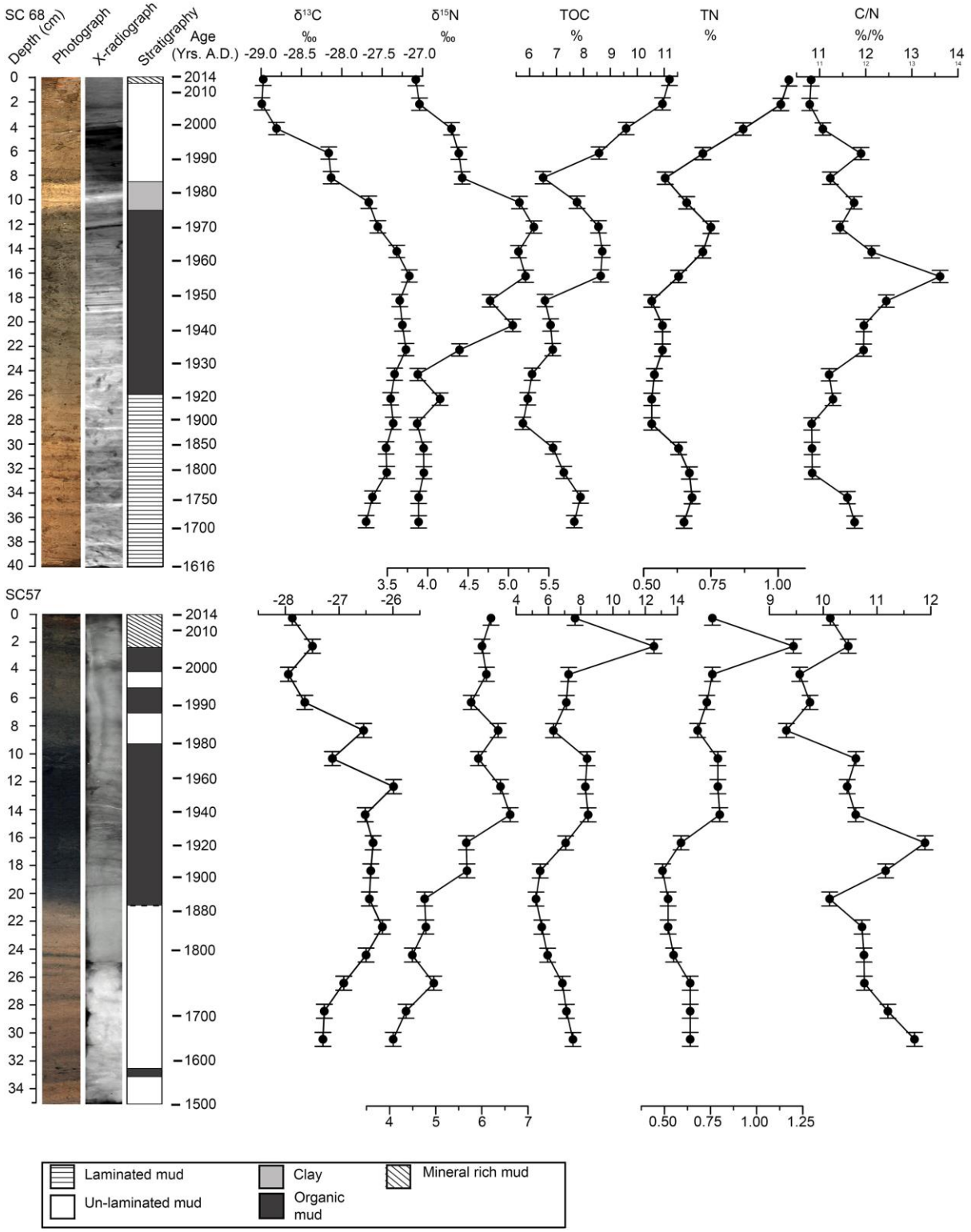

1025

1026

1027 Figure 6

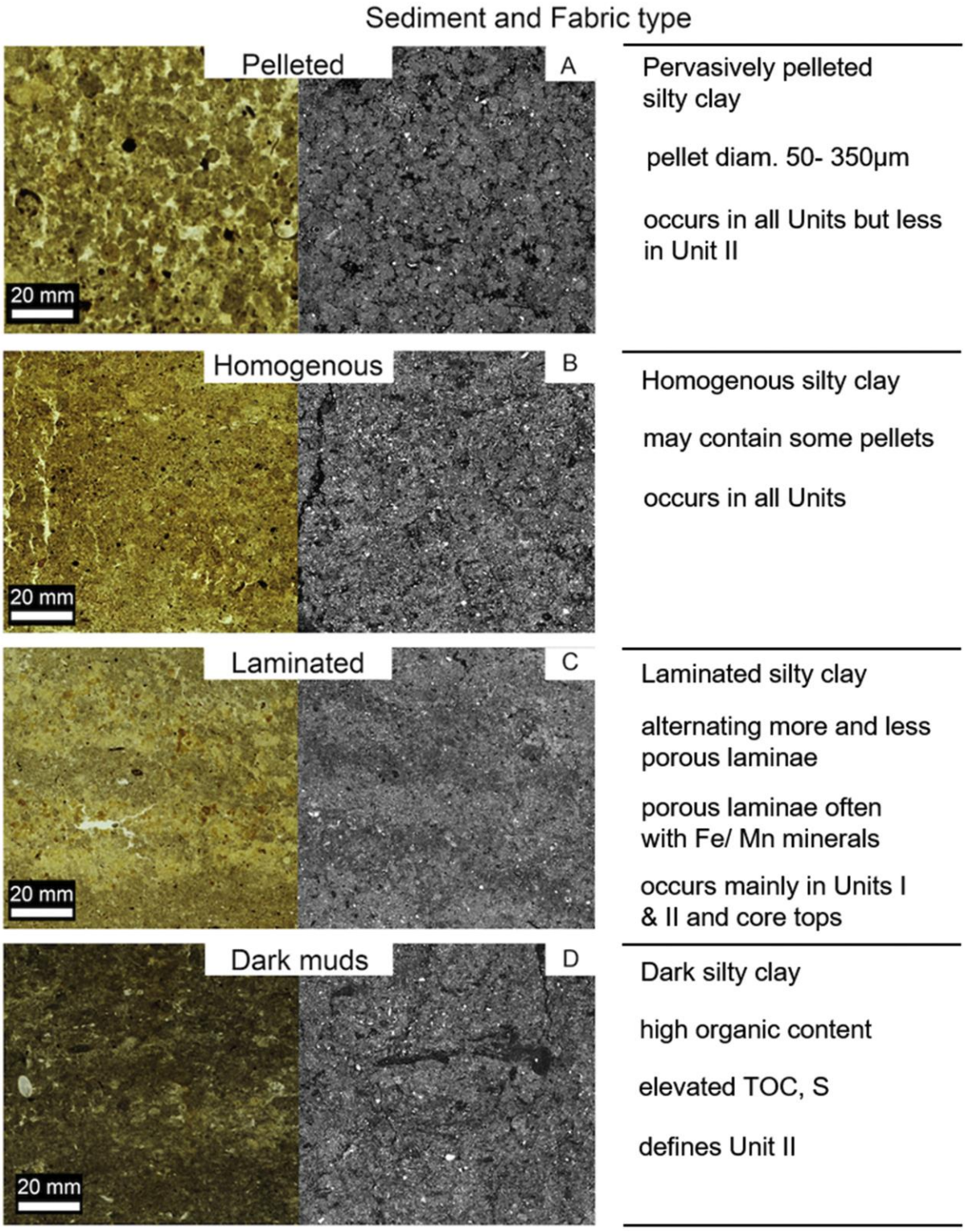

1028

1029

1030 Figure 7

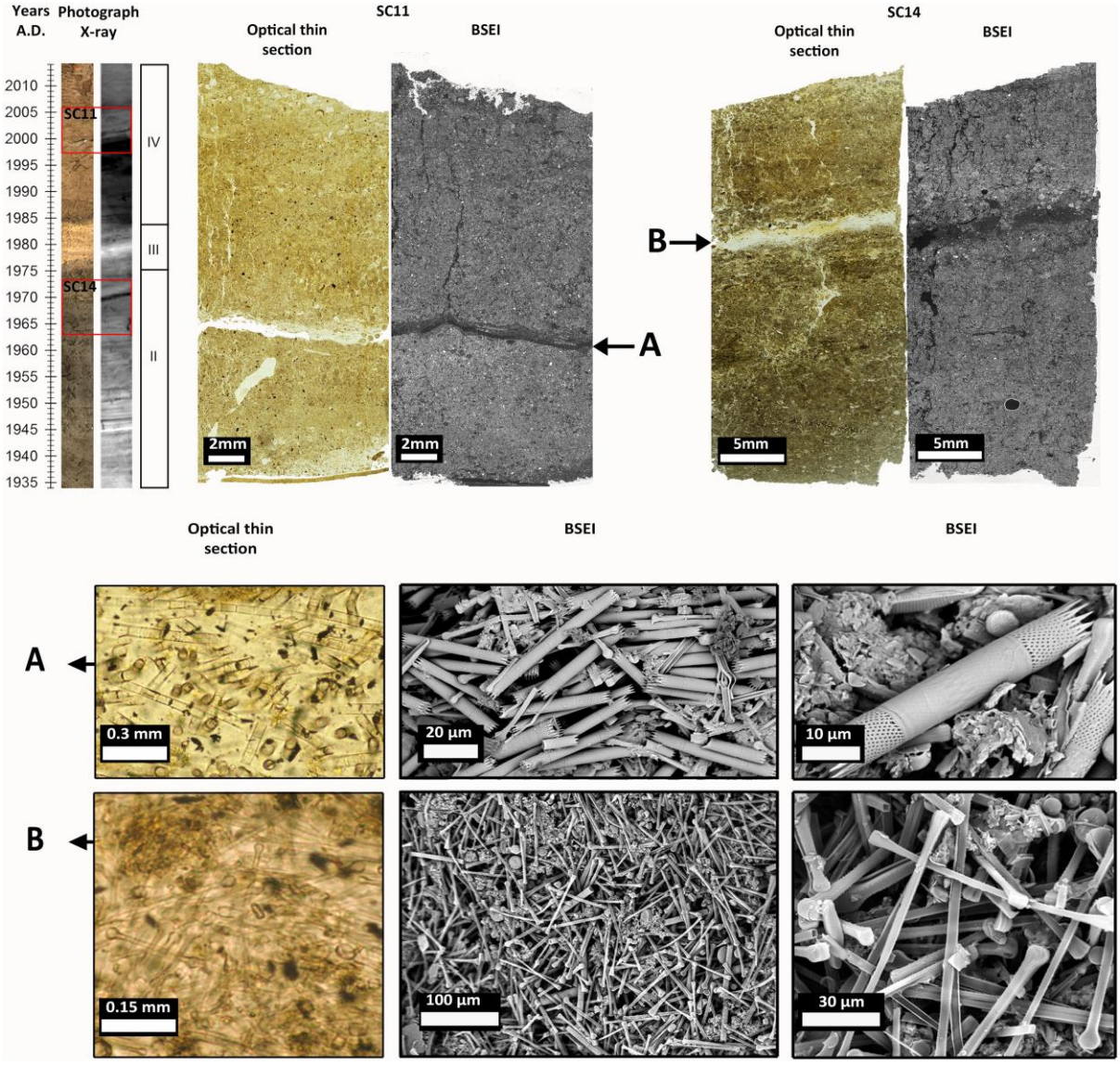

1031

1032

1033 Figure 8

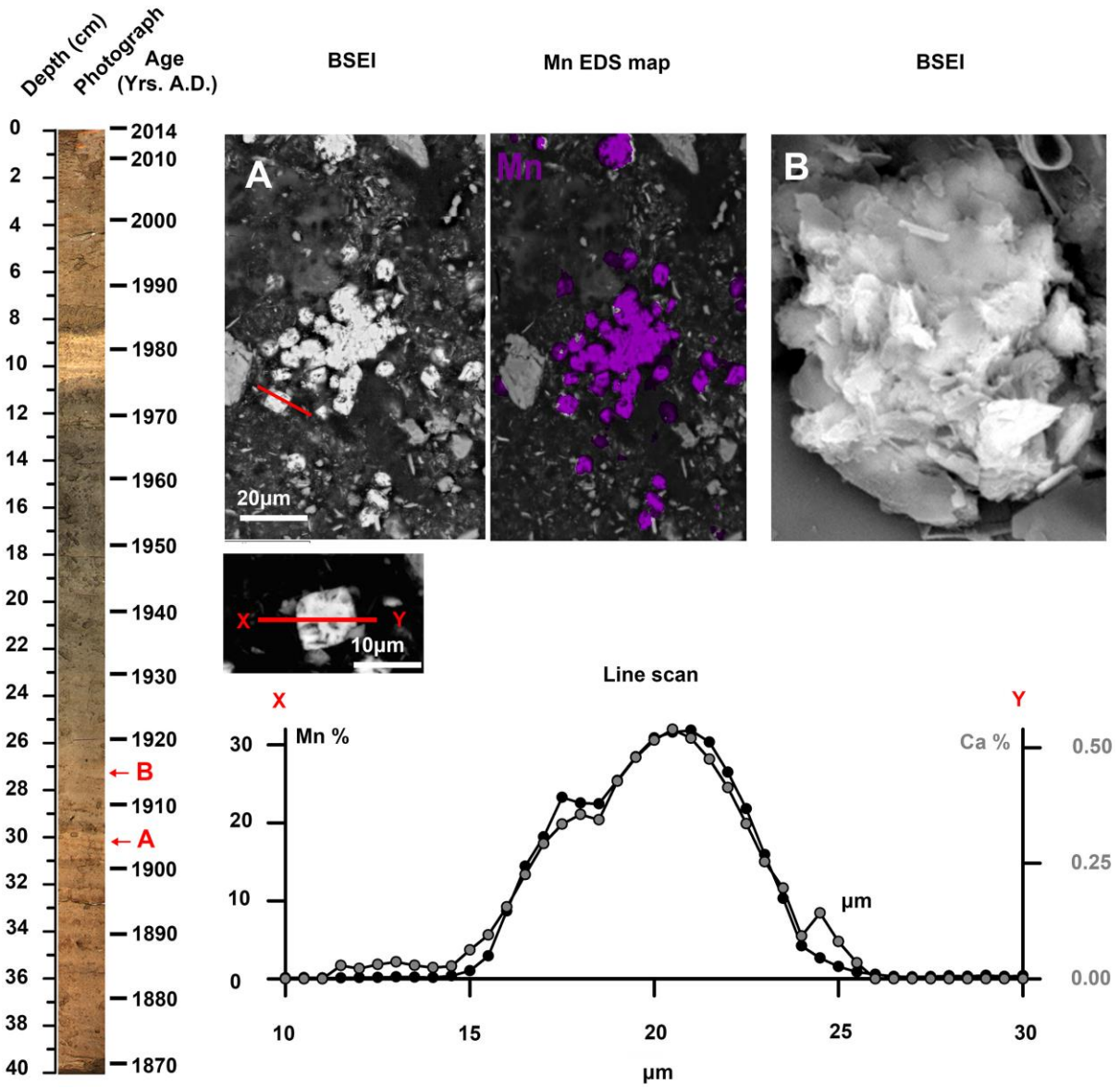

1034

1035

1036 Figure 9

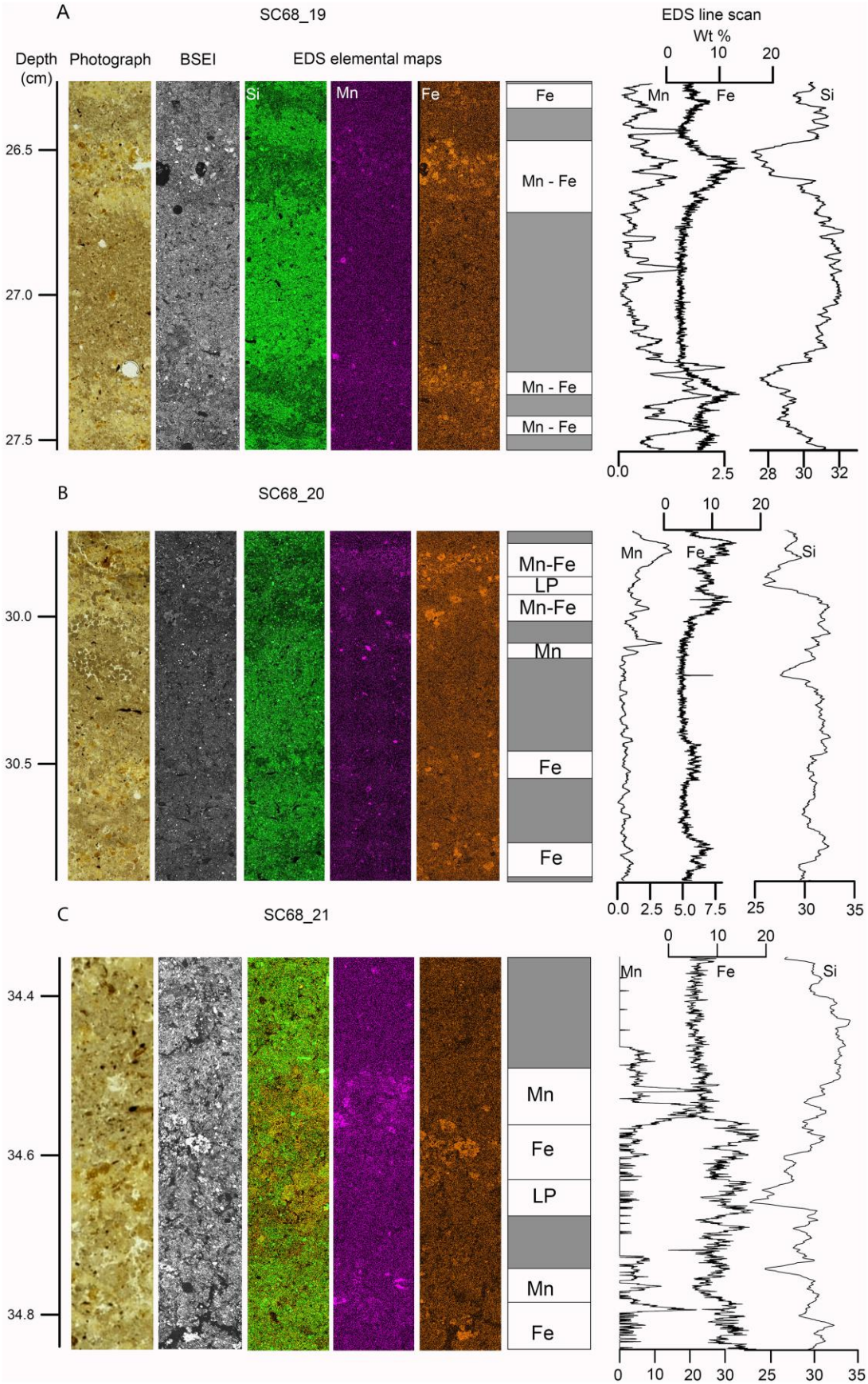

1037

1038

1039 Figure 10

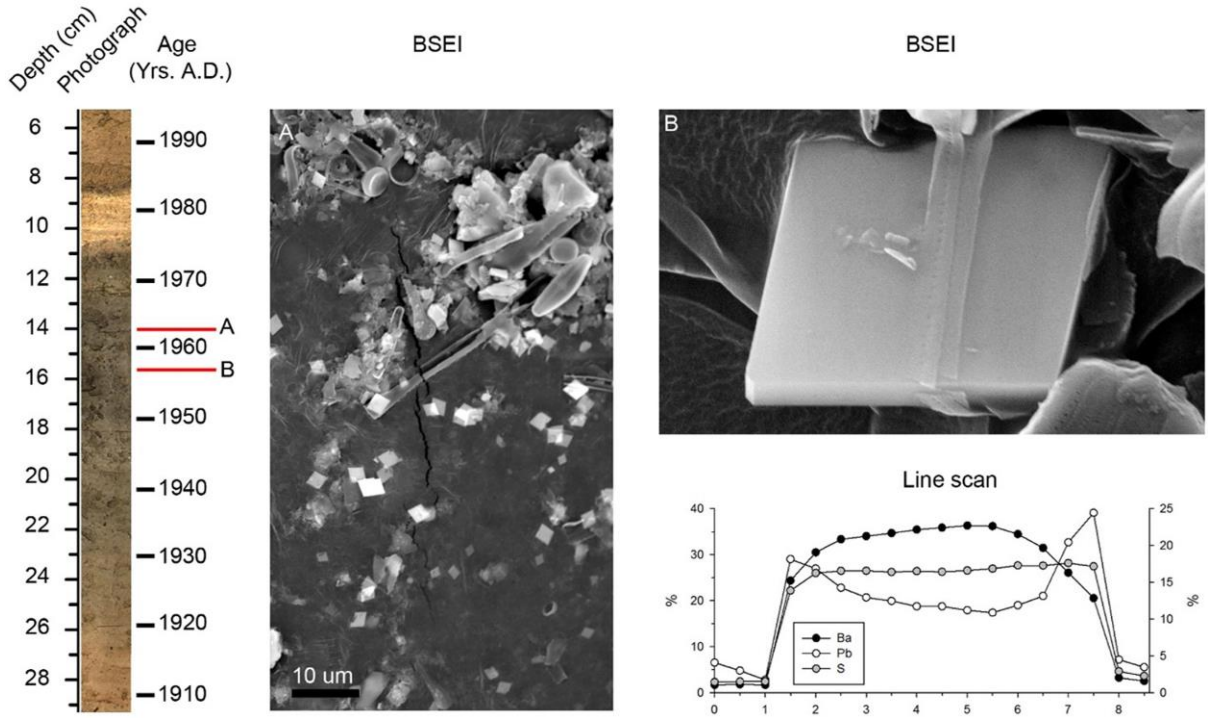

1040

1041

1042 Figure 11

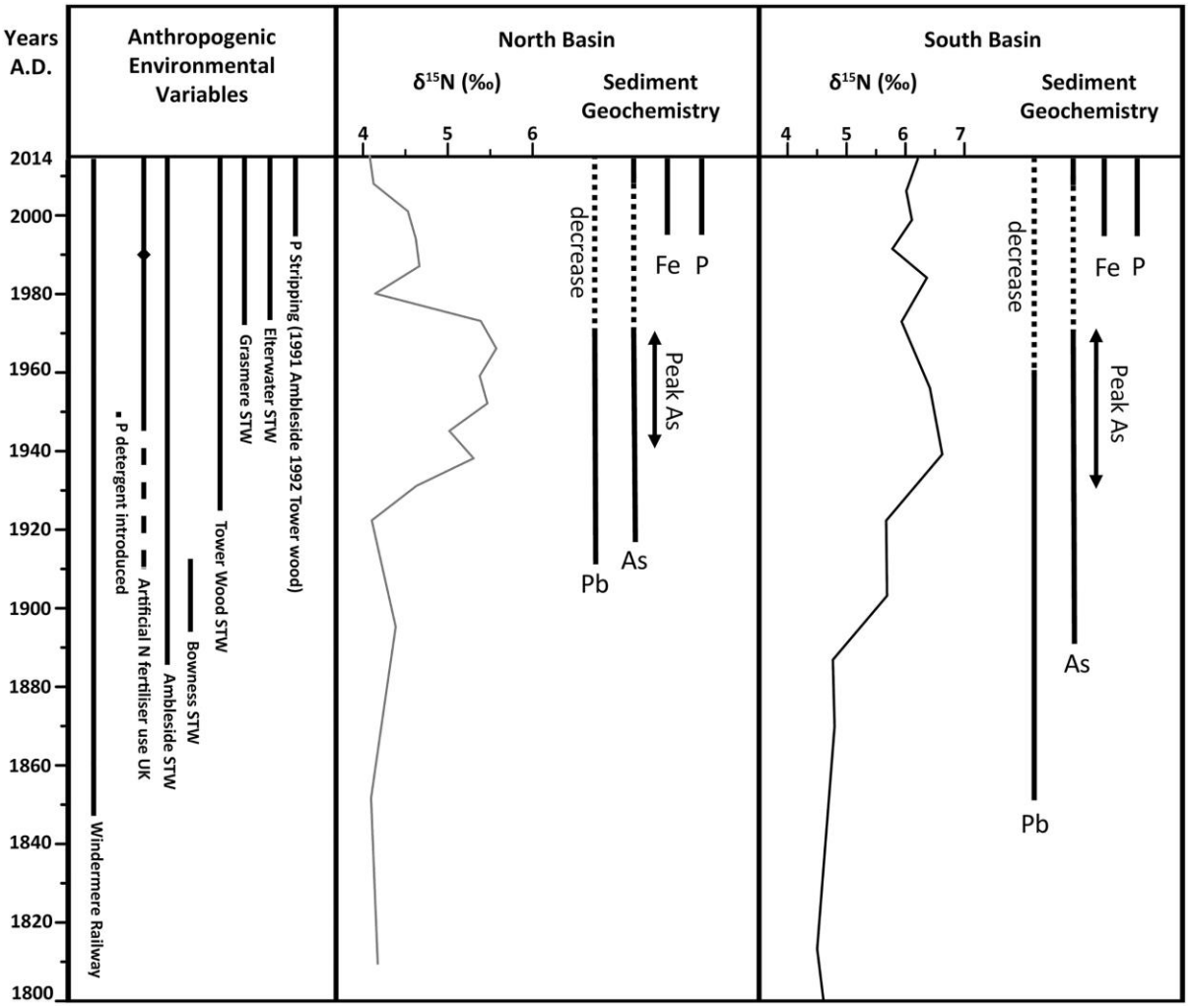

1043

1044

1045 Figure 12

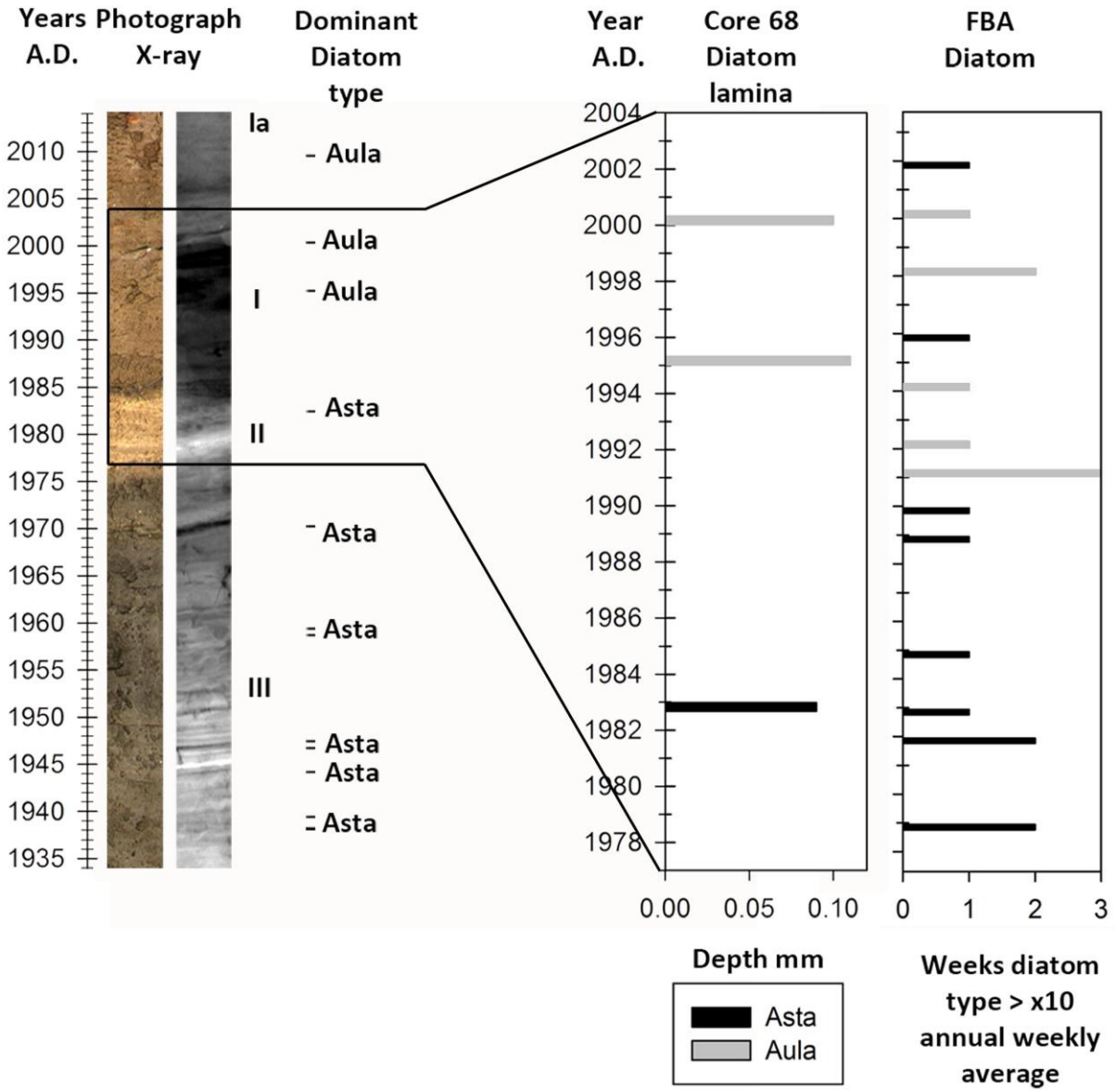

1046

1047

1048 Figure 13

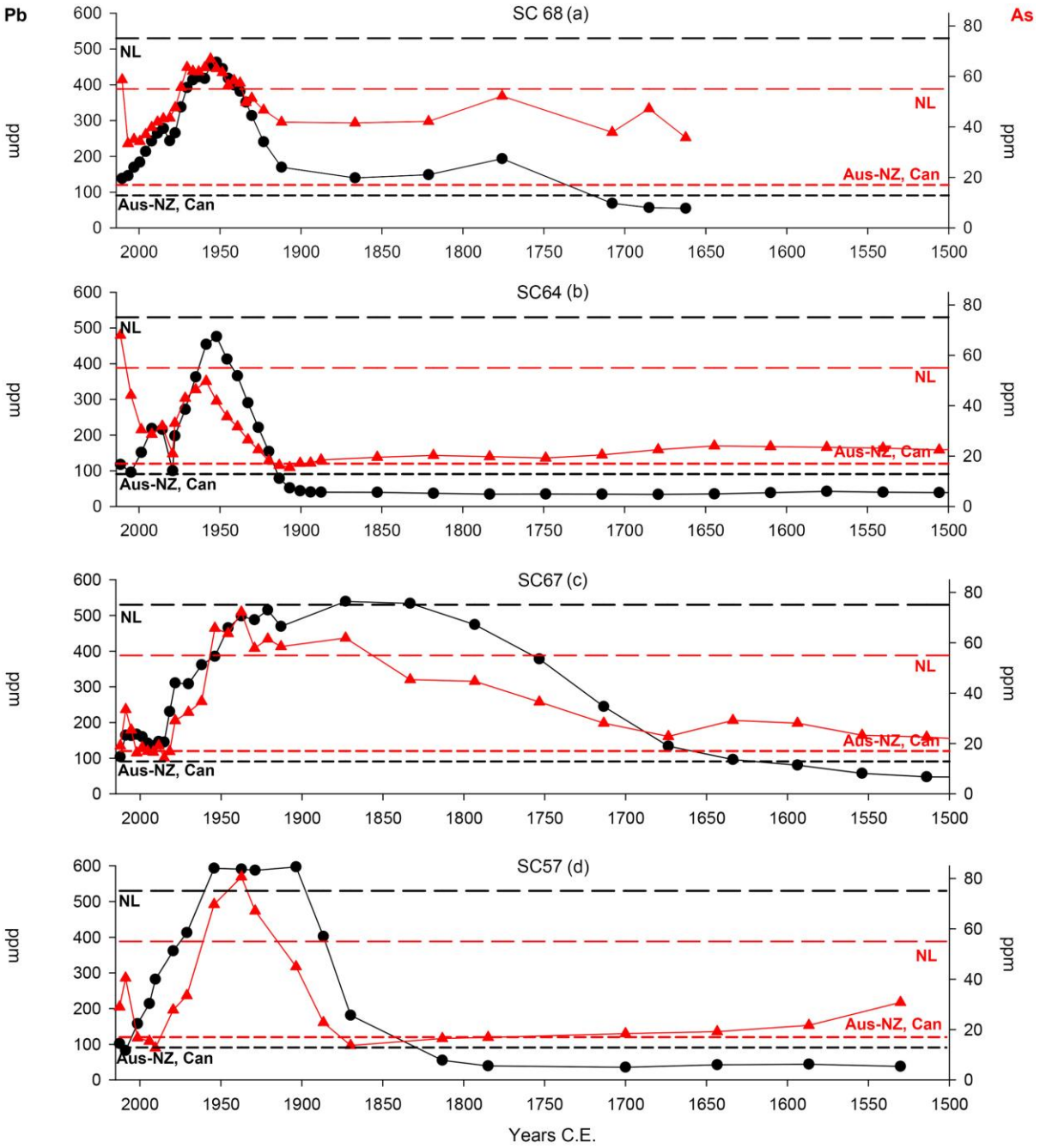

1049

1050

Table 1

Core	Location	Coordinates (UTM)	Water depth	Total length
SC68	Deep North Basin	502902, 6029135	53.9 m	40cm
SC64	Intermediate North Basin	504184, 6024639	26.1 m	35cm
SC67	Intermediate South Basin	503764, 6020856	29 m	30.5cm
SC57	Deep South Basin	503288, 6018757	39.1 m	35cm

Table 2

Core	Depth	Sample type	Mean Age Yrs. B.P.	2σ calibrated ages
68	69.5	bulk	1020	1109 - 1125
64	92	leaf	2544	2363-2620
67	48	twig	1214	1083-1160
57	78	wood	1651	1554-1732

Supplementary material for:

Tracing lake pollution, eutrophication and partial recovery from the sediments of Windermere, UK, using geochemistry and sediment microfabrics

J. James Fielding[1, 3], Ian W. Croudace[1], Alan E. S. Kemp[1], Richard B. Pearce, Carol J. Cotterill[2], Peter Langdon[3], Rachael Avery[1, 4]

[1]Ocean and Earth Science, University of Southampton, National Oceanography Centre, Southampton, SO14 3ZH, United Kingdom

[2]British Geological Survey, Lyell Centre, Research Avenue South, Edinburgh, United Kingdom EH14 4AP

[3] School of Geography and Environmental Science, University of Southampton, University Road, Southampton, SO17 1BJ

[5]Department of Geological Sciences, Stockholm University, SE-10691, Stockholm, Sweden

*corresponding author (jj1n19@soton.ac.uk)

6. Supplementary material

6.1. Detailed methods

6.1.1. Coring and location

Following the bathymetric surveys outlined in Miller et al. (2013 cores were taken with a Uwitec 86 mm diameter gravity corer over one day using two small vessels. On recovery sodium polyacrylate was used to solidify the water and preserve the water-sediment interface (WSI), a simple log was then taken before transport to the British Ocean Sediment Core Facility (BOSCORF).

6.1.2. Initial sampling and core logging

Digitally imaging was done using a Geotek™ Multi Sensor Core Logging-Core Imaging System (MSCL-CIS) and X-rayed. Slab samples were taken continuously with overlapping

sections for microfabric studies. The 1 cm-thick slabs were further X-rayed using a Hewlett Packard Faxitron X-radiography cabinet at 35 kVe for 10 seconds.

6.1.3. Microlithostratigraphy

To complement geochemical analyses, changes in the sediment microfabric were studied. Following sub sampling, slabs underwent fluid-displacive resin embedding after which covered thin sections (CTS) for optical microscopy and polished thin sections (PTS) for backscatter electron imagery were prepared. PTS were imaged and analysed using a Carl Zeiss LEO 1450VP Scanning Electron Microscope (SEM).

6.1.4. Geochemical analysis

6.1.5. Itrax XRF Core scanning

The core archive-half surface was analysed using an itrax XRF core scanner that incorporates and Energy Dispersive X-Ray Fluorescence analysis (ED-XRF) system (Croudace et al., 2006) with a step size of 200 µm. Data points were excluded from the analysis where surface discontinuities (e.g. cracks etc) led to reduced count rates. Data points with zero validity or a mean standard error of >5 were also excluded from analysis following recommended procedures. Elemental data (counts) was normalised by dividing it by total kilocounts per second (kcps) for each interval to account for changes in the core density and surface high between sample points and cores (Croudace et al. 2006).

6.1.6. Wavelength Dispersive XRF

In order to calibrate and complement the ED-XRF semi-quantitative itrax analysis, continuous 1 cm–thick homogenised bulk samples were analysed to produce fully quantitative results using a Philips Magix-Pro Sequential Wavelength Dispersive XRF Spectrometer WD-XRF (Almelo – Holland), with a 4 kW rhodium anode X-ray tube.

6.1.7. SEM-based energy dispersive X-ray microanalysis

The EDS instrumentation for elemental microanalysis was an Oxford Instruments X-Act 10mm^2 area Silicon Drift Detector, coupled with the AZtec Energy software system (v.3.1). Line scans were run at 20 kV, a WD of 19 mm, and a dwell time per analysis site of 60 seconds, with EDS data collected at ~5,000 cps. The calculated data have been acquired using standardless analysis, hence all results are normalized to 100%. Minimum detection limits are 0.195% for Na Kα and decreasing to 0.085% for Ca Kα (Goldstein et al., 2003).

6.1.8. TOC, TN, $\delta^{13}C$

SC68 from the North Basin and SC57 from the South Basin were analysed for TOC, TN, δ13C. 1 g samples were taken continuously at 2 cm intervals and freeze dried for 48 hours. Between 13 to 15 mg were taken from 6 samples representing end member sediment types in both cores were analysed for calcium carbonate ($CaCO_3$) content at the University of Southampton on AutoMate + CM5015 coulometer. All samples were analysed for TOC, TN, $\delta^{13}C$ using a Elementar Vario Isotope Cube Elemental Analyser equipped with a TCD (Thermal conductivity detector) which is interfaced with an Isoprime 100 continuous flow isotope ratio mass spectrometer (IRMS). Acetanilide was used as an elemental standard for C and N and USGS40 and USGS41 as international reference materials for the normalisation of the isotope ratios.

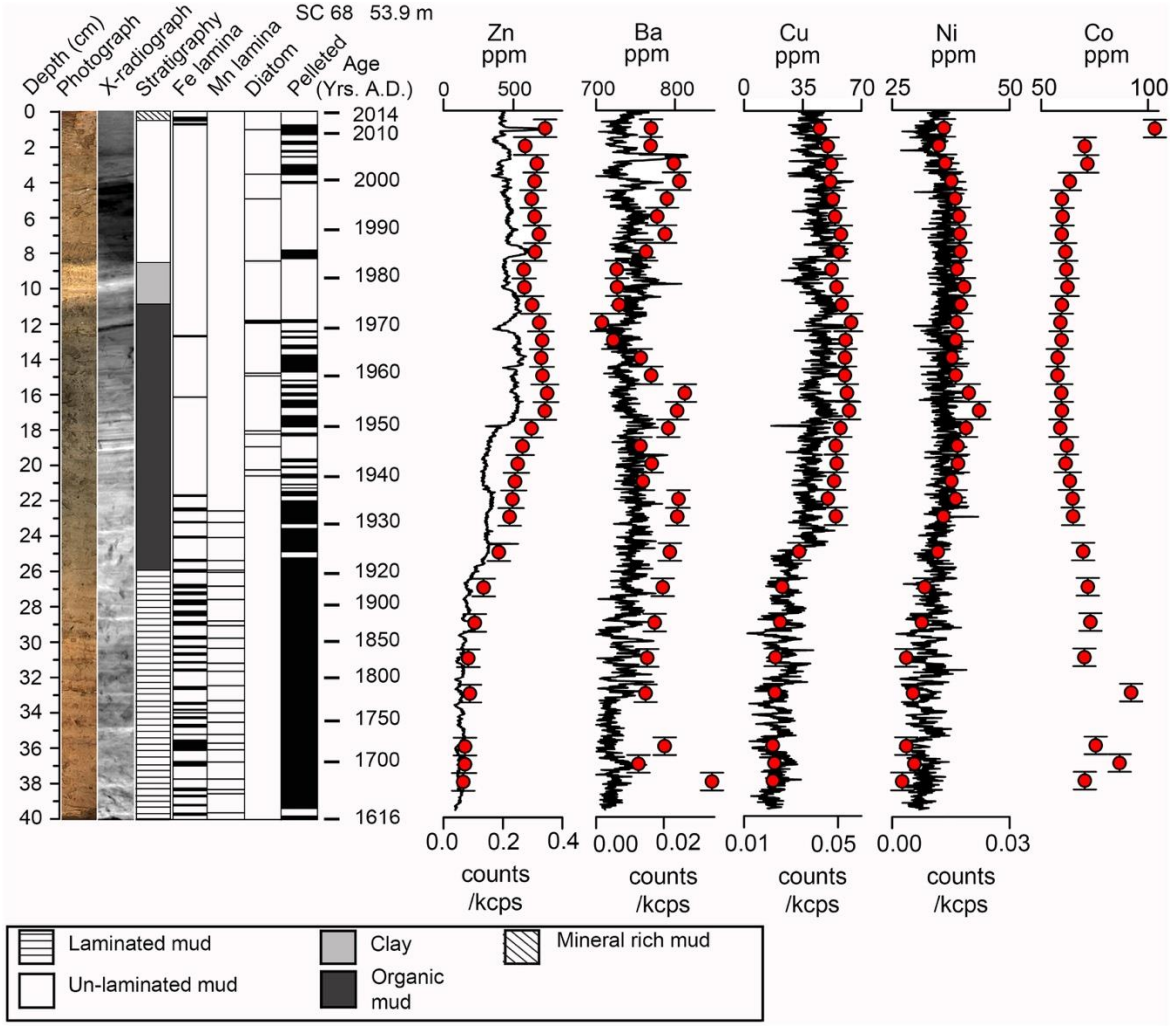

Supplementary Fig. 1.
Stratigraphy and geochemistry for SC68. Core depth in cm, core photograph, core x-radiograph, lithostratigraphy, sediment fabric types, ^{210}Pb CF:CS LSAR age depth model for the North Basin gravity cores. For geochemistry black lines show Itrax ED-XRF Zn, Ba, Cu, Ni and Co (lower scale). Red dots show discreet WD-XRF data for Zn, Ba, Cu, Ni and Co (titles in brackets, upper scales). Vertical errors on WD-XRF show the sampling interval. Water depths of each coring site are shown above the corresponding core.

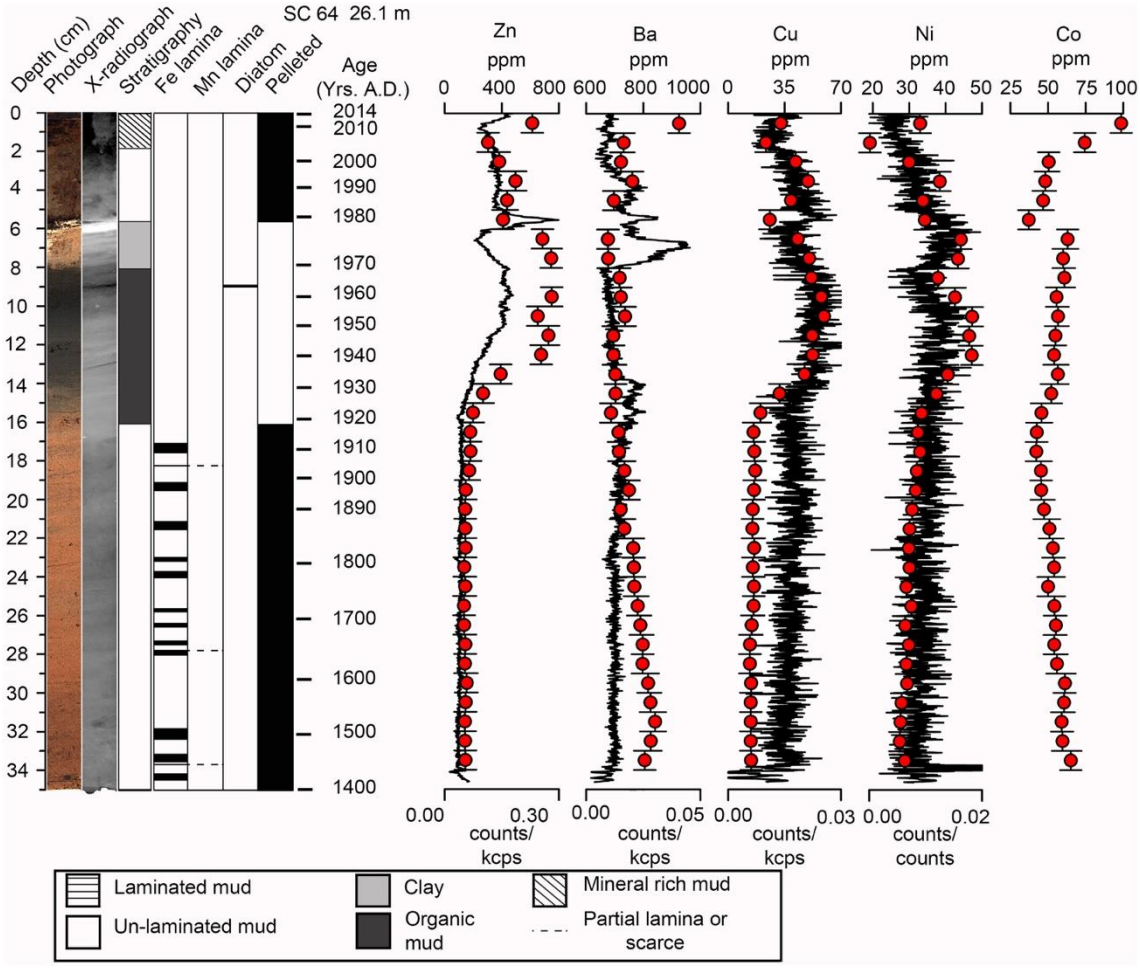

Supplementary Fig. 2.
Stratigraphy and geochemistry for SC64. Core depth in cm, core photograph, core x-radiograph, lithostratigraphy, sediment fabric types, ^{210}Pb CF:CS LSAR age depth model for the North Basin gravity cores. For geochemistry black lines show Itrax ED-XRF Zn, Ba, Cu, Ni and Co (lower scale). Red dots show discreet WD-XRF data for Zn, Ba, Cu, Ni and Co (titles in brackets, upper scales). Vertical errors on WD-XRF show the sampling interval. Water depths of each coring site are shown above the corresponding core.

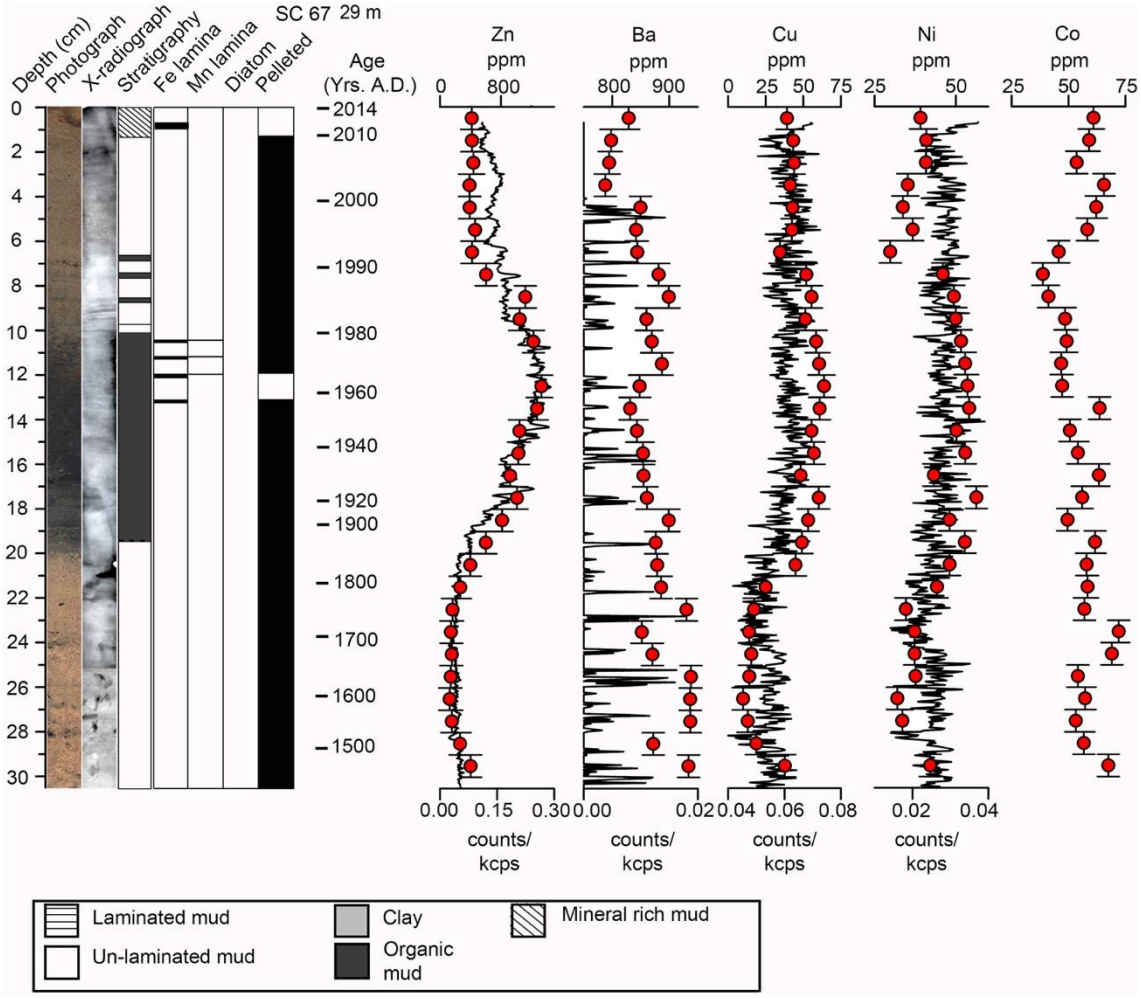

Supplementary Fig. 3.
Stratigraphy and geochemistry for SC67. Core depth in cm, core photograph, core x-radiograph, lithostratigraphy, sediment fabric types, ^{210}Pb CF:CS LSAR age depth model for the North Basin gravity cores. For geochemistry black lines show Itrax ED-XRF Zn, Ba, Cu, Ni and Co (lower scale). Red dots show discreet WD-XRF data for Zn, Ba, Cu, Ni and Co (titles in brackets, upper scales). Vertical errors on WD-XRF show the sampling interval. Water depths of each coring site are shown above the corresponding core.

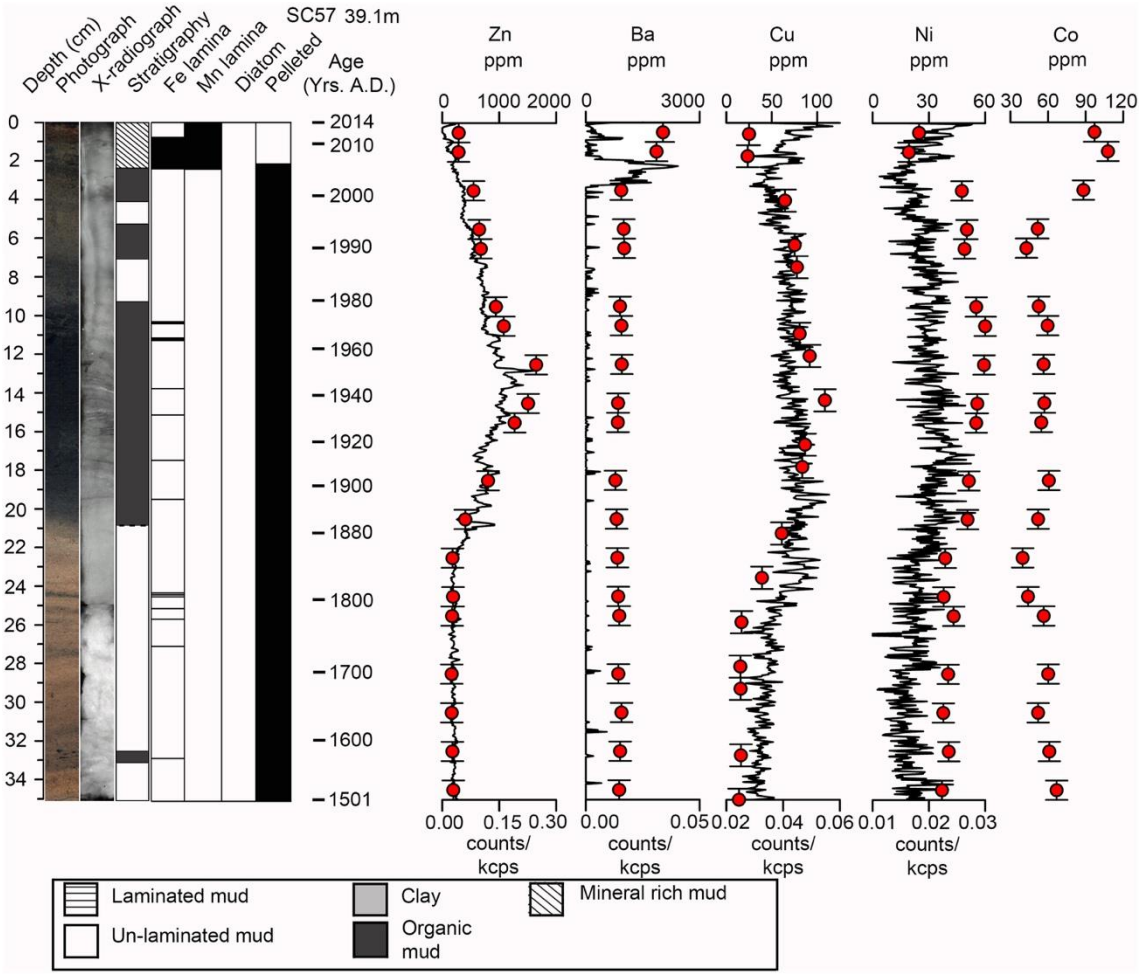

Supplementary Fig. 4.
Stratigraphy and geochemistry for SC57. Core depth in cm, core photograph, core x-radiograph, lithostratigraphy, sediment fabric types, ^{210}Pb CF:CS LSAR age depth model for the North Basin gravity cores. For geochemistry black lines show Itrax ED-XRF Zn, Ba, Cu, Ni and Co (lower scale). Red dots show discreet WD-XRF data for Zn, Ba, Cu, Ni and Co (titles in brackets, upper scales). Vertical errors on WD-XRF show the sampling interval. Water depths of each coring site are shown above the corresponding core.